Chapter 2

Fabrication, Characterization and Modification Strategy of Electrospun Nanofibrous Scaffolds from Acid and Alkaline Hydrolyzed Gelatin for Corneal Tissue Engineering

2.1 Introduction

Gelatin is a natural protein biopolymer extracted and acquired from partial hydrolysis of native collagen. Collagens are the most abundant naturally occurring structural protein present in almost all parts of the animal body i.e., bone, cartilage, and skin, cornea, tendon, and ligaments (Z. Zhang et al. 2013; Aramwit et al. 2015; Yin-Guibo et al. 2009). Gelatin is reported to contain 18 amino acids partially linked to each other. Figure 2.1 depicts the basic chemical structure of gelatin.

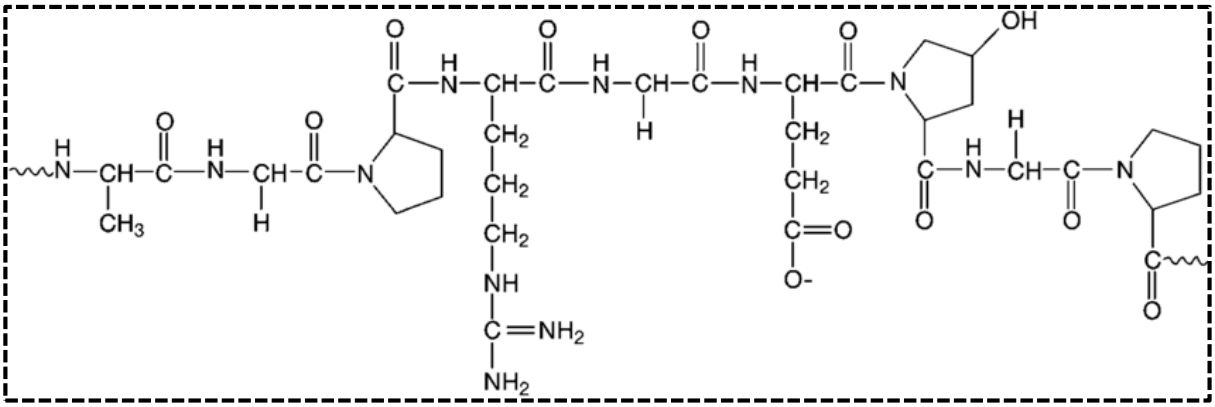

Figure 2.1 Basic chemical structure of gelatin (Kommareddy, Shenoy, and Amiji 2007).

Glycine is one of the three predominant amino acids in the gelatin molecule that modulates cell adhesion (Alihosseini 2016; Barchuk et al. 2016; Massoumi et al. 2016) (Figure 2.2). Partial hydrolysis of collagen could be performed either by physical, chemical or thermal denaturation (Barchuk et al. 2016). Gelatin has been classified into two types i.e. acid hydrolyzed gelatin (gelatin A) and base hydrolyzed gelatin (gelatin B) based on the acid or alkaline/base pre-treatment and thermal denaturation of collagen (Faradiella, Ningsih, and Triastuti 2017) (Figure 2.3). Gelatin type A (acid pre-treated) has broad isoelectric range between pH 7-9, while gelatin type B (basic pre-treated) has a narrow isoelectric range between 4.7- 5.4 (Okhawilai et al. 2010; Van Vlierberghe et al. 2014).

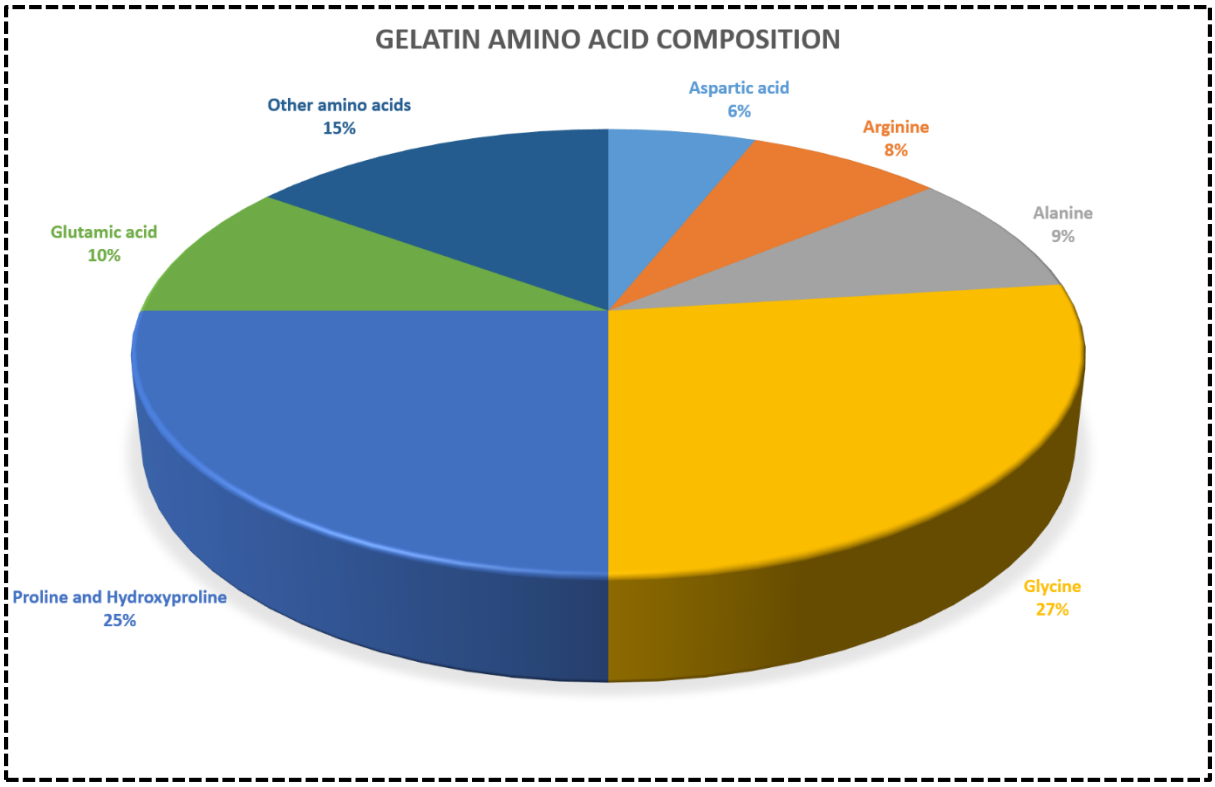

Figure 2.2 Basic amino acid composition of gelatin.

Glycine is present at a *N*-terminal of alkali processed gelatin while alanine is predominant in acid processed gelatin (Djagny, Wang, and Xu 2001). Acid hydrolyzed gelatin (GA) contains higher elastic modulus as well as viscosity compared to base hydrolyzed gelatin (GB), rendering them preferable for tissue engineering applications (Table 2.1).

Many similar characteristics from native collagen and low cost of the gelatin proteins make it preferable to be used for scaffold fabrications in tissue engineering applications (Mohiti-Asli and Loboa 2016; Deshmukh et al. 2017). Gelatin has wide spectrum applications such as gelling agents in food industry, gelatin desserts, gummy candies, ice creams, dips, yogurts, and marshmallows. Moreover, these are used in photographic films, papers cosmetics and various pharmaceutical and medical fields such as hard and soft capsules/microcapsules, drug delivery carriers (e.g. microspheres), sealants for vascular prosthesis, drugs, wound healing dressings

and multivitamin capsules (Massoumi et al. 2016; Deshmukh et al. 2017; Moreno and Peinado 2012; Bandyk et al. 2001; Land, Piehl, and Burks 2013; Ramos et al. 2016; Hajikarimi and Sadeghi 2020; Ji et al. 2018).

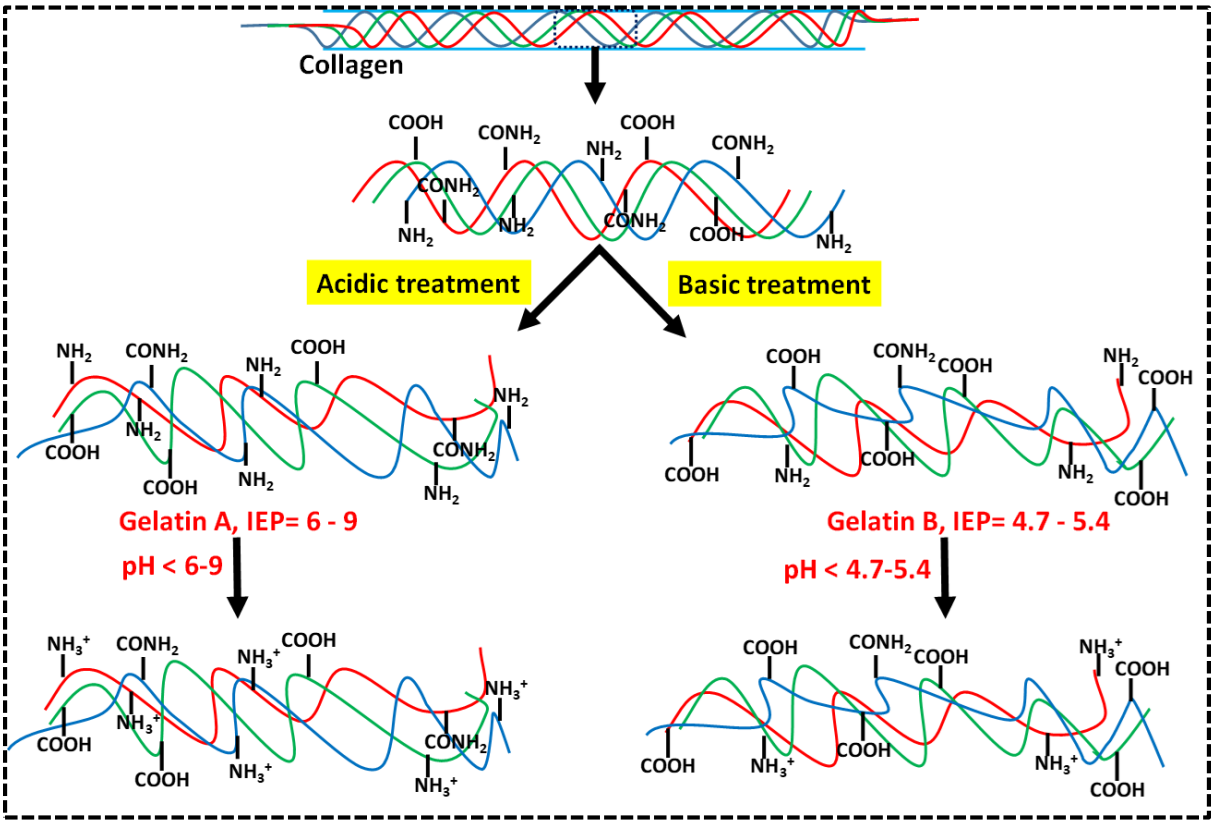

Figure 2.3 Preparation of two distinct gelatins from collagen hydrolysis by acidic and basic treatments (Wahab and Mahat 2016).

Several advantages such as non-immunogenicity, biodegradability and biocompatibility make it a suitable candidate for biomedical applications (Yin-Guibo et al. 2009). Nowadays, due to their versatile nature these biopolymers have widened their applications in various other areas of biomedical and tissue engineering. Gelatin is well known for its film-forming properties that enable it to draw in sheets and cell adhesion substrates (Salvatore et al. 2012). There are few limitations with film based scaffolds and substrates i.e. low surface area-to-volume ratio, poor porosity, and mechanical strength (Barchuk et al. 2016; Ramos et al. 2016; Ji et al. 2018). To

overcome these limitations, gelatin electrospinning approach could be applied which would ultimately lead to aligned/non-aligned nanofibrous scaffold with high porosity, increased surface-to-volume ratio and enhanced mechanical strength (Yin-Guibo et al. 2009; Barchuk et al. 2016; Okhawilai et al. 2010; Choktaweesap et al. 2007; Dadras Chomachayi et al. 2018; Huda et al. 2017).

Table 2.1 Characteristics of gelatin type A and type B as described in the literatures (Kuijpers et al. 1999a; Lee et al. 2016).

Properties/Characteristic	**Gelatin Type A**	**Gelatin Type B**
Treatment	Hydrochloric acid/Acid	Sodium Hydroxide/Lime water
pH	4.5 – 6.0	5.0 – 7.0
Isoelectric Point	7.0 – 9.0	4.8 – 5.4
Gel Strength (Bloom)	300	150 – 250
Ash	0.3 – 2.0	0.5 – 2.0
Net charge at physiological pH	Positively charged	Negatively charged
Biocompatibility	Fair	Good
Viscosity (millipoise)	Partially higher	Partially lower
Degree of crosslinking	Low	High
Elasticity modulus	High	Low
Free carboxylic group	Low	High
Characteristic amino acids	Asparagine, Glutamine	Aspartic acid, Glutamic acid
Molecular weight (kDa)	50000-100000	90000-100000

Gelatin nanofibrous scaffolds could be a potentially advantageous candidate to mimic the extracellular matrix (ECM) as well as for developing nanoporous wound dressing, and

sustained-release drug delivery system (Jang et al. 2018; Foox and Zilberman 2015). However, gelatin based electrospinning approach is difficult with water based solution; therefore it requires a highly polar, volatile, organic solvent or a mixture of two or more solvents to enable its electrospinning behavior (Mohiti-Asli and Loboa 2016; Song, Kim, and Kim 2008). There are various solvents such as trifluoroethanol (TFE), acetic acid, and formic acid, which could be used to fabricate controlled gelatin nanofibrous scaffolds.

Silk fibroin (SF) is a naturally occurring, biocompatible, highly stable and mechanically robust polymeric biomaterial that is known to have wide applications in tissue engineering and regenerative medicines (Qi et al. 2017; Lawrence et al. 2009; Singh, Bandyopadhyay, and Mandal 2019; Li et al. 2017; Chen et al. 2019). SF is generally isolated from cocoons of silkworm (e.g. *Bombyx mori*) and is well known for its transparency, non-toxicity, tuneable mechanical property, low immunogenicity, oxygen and water vapour permeability and naturally crosslinking property. Silk could be molded into arrangements that could enable various optical based applications e.g. lensing and diffraction devices, non-linear optical behaviours, and wave guiding (Kujala et al. 2016; Lawrence et al. 2008; Rice et al. 2008). Cell growth and proliferation are slightly lower on SF scaffolds due to limited number of cellular adhesive sequences (e.g., RGD) (Chen et al. 2019; Guidetti, Wang, and Omenetto 2020; Tran, Wilson, and Seib 2018; Aziz et al. 2017).

Among biomaterials, gelatin could be employed to fabricate cornea, as it is the hydrolyzed derivative of collagen, which is the major composition of cornea. Gelatin is a popular biopolymer because of its inexpensiveness, biocompatibility and biodegradable nature. Moreover, gelatin is devoid of any harmful/toxic effect on the cells and supports the growth, development and proliferation of cells (Farasatkia et al. 2021; Mohammadzadehmoghadam

and Dong 2019). The limitations of gelatin biopolymers are its high degradability and instability on long-term incubation under physiological aqueous environment. Stabilization of gelatin nanofibrous scaffolds may be accomplished in two ways: through crosslinking or via composite reinforcement. Chemical cross-linkers (i.e., glutaraldehyde, 1-ethyl-3-(3-dimethylaminopropyl) carbodiimide / N-hydroxysuccinimide) EDC/NHS) could serve as stabilizing agents, but have certain limitations such as cytotoxicity and pro-inflammatory effects on macrophage-like cells, which negatively affect the biocompatibility of chemically cross-linked scaffolds (Hussein et al. 2017). Composite reinforcement adds rigidity and strength to a structure, which allows it to withstand structural loads. Composite materials retain their own identities while maintaining a relationship between their characteristics and the product produced by their combination (Tripathi 2017). Therefore, in this chapter we adopted composite reinforcement technique to stabilize gelatin nanofibrous scaffold.

Electrospinning approach could be ideal for fabricating corneal stromal equivalents mimicking corneal architecture (Tonsomboon and Oyen 2013). In this presented work, we have used a ternary solvent (glacial acetic acid/ethyl acetate/water) to solubilize gelatin of both types (i.e. A and B) separately, fabricated electrospun nanofibers using the prepared gelatin solutions and characterized the scaffolds based on various parameters including scanning electron microscope (SEM) analysis, porosity, water retaining capacity, attenuated total reflection-Fourier transform infrared (ATR-FTIR) analysis, and in vitro degradation of the fabricated nanofibrous scaffolds. Additionally, to maintain the stability of gelatin-based scaffolds under physiological circumstances, silk fibroin was penetrated inside the nanofibrous scaffolds followed by their physically crosslinking via ethanol vapor treatment. The scaffolds were then characterized for various parameters, including scanning electron microscopy (SEM) analysis,

porosity, water-retention capacity, transparency, and attenuated total reflection-Fourier transform infrared (ATR-FTIR) analysis. To explore the possibility of its application in corneal tissue fabrication, we have also assessed the cellular compatibility using corneal fibroblast cells.

2.2 Materials and method

2.2.1 Materials

Gelatin A (Bloom strength 300, molecular weight distribution: 50000-100000 Da) was procured from Sigma Aldrich. Gelatin B (Bloom strength 250, molecular weight distribution: 90000-100000 Da) was purchased from HiMedia, India. Dialysis membrane [12,000 molecular weight cut off (MWCO)], polyethylene glycol (PEG, molecular weight- 20,000), lithium bromide (LiBr), phosphate buffer saline (PBS), 3-(4,5-dimethyl-2-thiazolyl)-2,5-diphenyl-2H-tetrazolium bromide (MTT), Dulbecco's modified Eagle's medium (DMEM) high glucose, fetal bovine serum (FBS), antibiotics penicillin and streptomycin solution (100X) were purchased from HiMedia, India. Absolute ethanol 99.9% of high analytical grade and distilled water were used in all the experiments. Glacial Acetic Acid (GAA), ethyl acetate, sodium carbonate (Na_2CO_3) were procured from SRL, India.

2.2.2 Methods

2.2.2.1 Fabrication of electrospun gelatin nanofibrous mats

Gelatin A and gelatin B solutions were prepared separately using a ternary solvent (glacial acetic acid/ethyl acetate/deionized water) in a ratio of 4.2:2.1:1 w/w respectively (10% w/w) (Tonsomboon and Oyen 2013). The solutions were stirred for 2 h at 1000 rpm, 40°C on the hot plate. The solutions were cooled down to the room temperature before performing the electrospinning. Super ES-2 electrospinning unit from E-Spin Nanotech Pvt. Ltd., India was

used to fabricate nanofibrous sheets. Various parameters such as flow rate, sample concentration, applied voltage and the distance between the needle and collector were selected with multiple values while optimizing for nanofiber formation. Most of the values such as sample concentration, sample solvents, and distance between needle and collected were cited from Tonsomboon et al., (Tonsomboon and Oyen 2013). Few parameters such as syringe volume and flow rate were already provided in the user manual instructions of the instrument (espin nanotech, IIT Kanpur). Rest of the parameters such as applied voltage and thickness of the scaffold were optimized after multiple attempts. A summary of optimized parameters for electrospinning process is given in table in figure 2.4. Briefly, the solution was dispensed at a flow rate of 0.40 mL/h using a 10 mL luer lock syringe with a 21-gauge needle.

Schematic for electrospinning setup

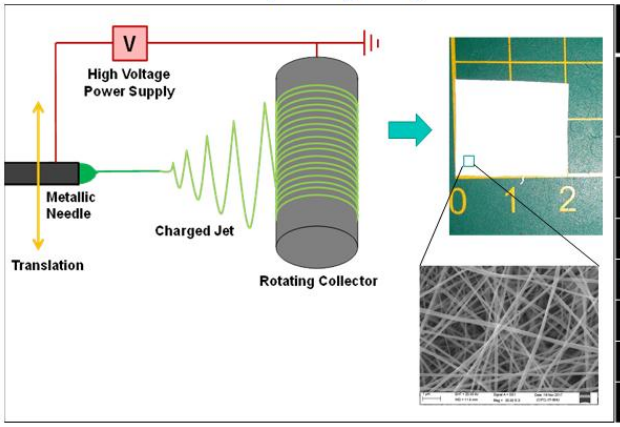

Optimized parameters for gelatin electrospinning

Parameters	Optimized Values
Distance between needle tip and collector	15 cm
Needle	21 gauge bevel tip needle
Flow rate	0.4 mL/h
Applied High voltage	15 kV
Syringe inner diameter	16 mm
Syringe volume	10 mL
Collector type	Rotating drum collector
Collector speed	1000 rpm

Figure 2.4 Depicts schematic for electrospinning setup and optimized parameters for gelatin electrospinning.

The drum collector was placed at 15 cm distance spinning at a rotation speed of 1000 rpm with an applied high voltage of 15 ± 1 kV for 36 h. The electrospun mats were further air dried in the laminar airflow chamber overnight to desiccate them completely.

2.2.2.2 Preparation of silk fibroin solution

Mulberry based cocoons from *Bombyx mori* were purchased from Research Extension (Silk Board), Bhadrasi, Varanasi, ministry of textiles, Government of India. Silk fibroin was isolated as described earlier (Rockwood et al. 2011). Briefly, larger cocoons were chopped into smaller pieces, which were further degummed using 0.02 M sodium carbonate (Na_2CO_3) for 30 minutes in boiling deionized water. The fibers isolated were rinsed thoroughly in hot water to remove most of the sericin content, followed by air drying at room temperature overnight. Furthermore, the extracted and dried silk fibers were solubilized in 9.3 M lithium bromide and incubated at 60°C for 4 h for the complete dissolution of the silk fibers. The silk fiber-containing solution was dialyzed using 12 k Da cellulose dialysis membrane at 4°C for 3 days against deionized water to remove lithium bromide completely (Figure 2.5).

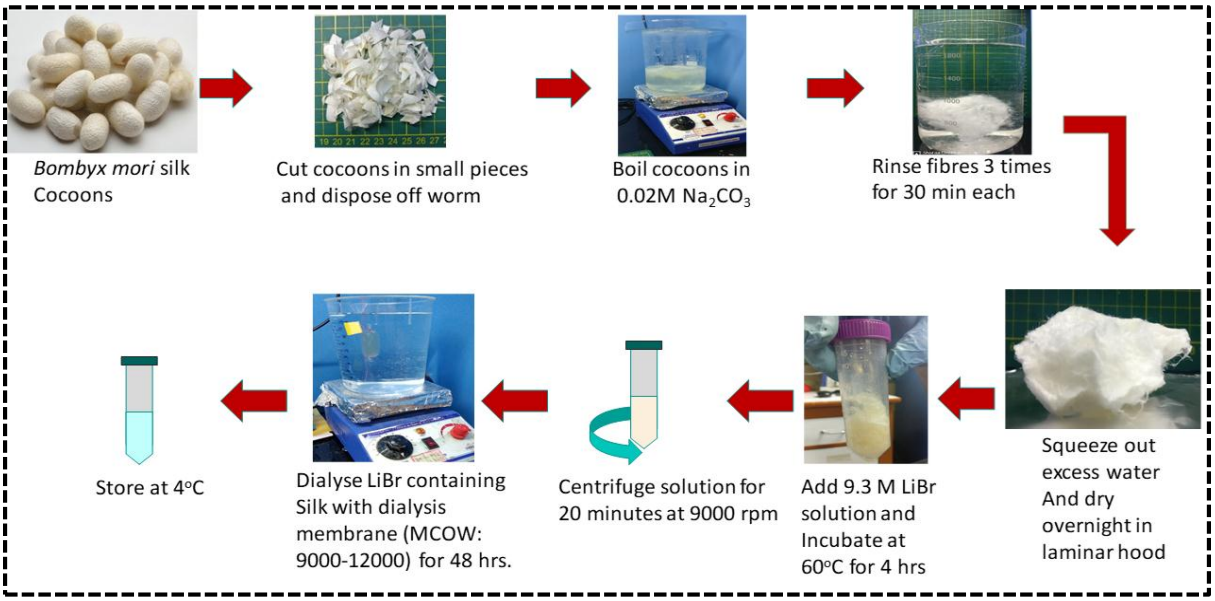

Figure 2.5 Schematic flow diagram for silk fibroin extraction procedure.

The water was regularly changed every 6 h to maintain the concentration difference for passive diffusion of lithium bromide outside from the dialysis bag. Thus, the obtained silk fibroin solution was around 7-8% (w/v) solution, which was however found difficult to spin coat due

to less viscosity. Therefore, the silk solution was again dialyzed against 10% (w/v) polyethylene glycol (MW. 20,000) for 10 h to obtain relatively more concentrated silk fibroin solution (14-16% (w/v)).

2.2.2.3 Silk permeation inside gelatin scaffold

Electrospun nanofibrous gelatin A scaffold was observed to degrade within 24 h in PBS at 37°C. To improve the integrity and stability of nanofibrous gelatin A scaffolds in culture medium, scaffolds were permeated with 14-16% w/v silk fibroin solution obtained from *Bombyx mori* as described earlier. Furthermore, the nanofibrous scaffolds permeated with silk fibroin (SFG) were treated with 70% ethanol vapor overnight for physically crosslinking the silk fibroin to stabilize the gelatin A nanofibers inside the scaffold. Briefly, the 60 mm Petri dish was placed in an inverted position on the spin coater chuck and silk fibroin solution was spin-coated at 500 rpm for 1 minute at an acceleration of 500 rpm/s to obtain a thickness around ~400-500 microns. Thickness was measured from microscopic images of the cross-sectional area from the obtained scaffold. Furthermore, the electrospun gelatin mat was placed on the top of spin-coated silk fibroin gently, which allowed permeation of silk fibroin in all the unoccupied space in-between the nanofiber space (figure 2.6a). The silk permeated mat was further air-dried overnight. Moreover, the scaffold was treated overnight with 70% ethanol vapor to physically crosslink the silk and to increase number of beta sheets formation (figure 2.6b). The fabricated scaffold was further characterized for its enhanced stability and cytocompatibility.

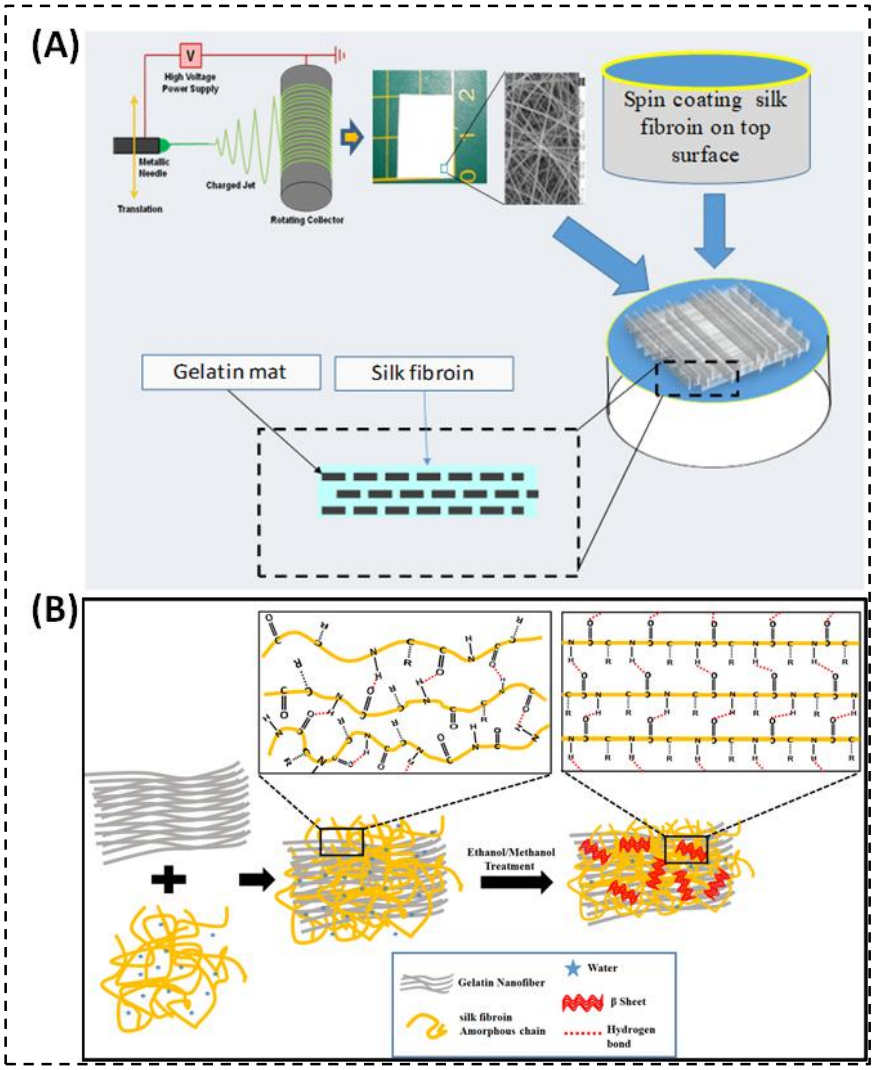

Figure 2.6 Schematic procedure for (A) silk permeation inside the electrospun gelatin A nanofibrous structure and (B) schematic representing ethanol vapor crosslinking of the silk permeated gelatin A nanofibrous (SFG) scaffold. Ethanol vapor treatment alters silk confirmation from least stable, high water soluble scaffold to highly stable, less water-soluble silk. Therefore, the gelatin nanofibers of silk permeated gelatin A (SFG) remains protected from fast degradation enhancing its stability under physiological conditions.

2.2.3 Characterization of the scaffolds

2.2.3.1 Morphological characterization of electrospun nanofibers

Scanning electron microscopic [Zeiss EVO 18 SEM Zeiss, (Germany)] images of the fabricated nanofibrous mats were characterized for their morphological features such as nanofibers arrangement, fiber size, the porous space in-between the nanofibers. Briefly, the 10

mm x 10 mm samples were sputter-coated with gold and were studied for their physical appearance at various magnifications. The SEM micrographs were captured at 3 different magnifications i.e., at 5k, 10k and 25k, at an accelerating voltages of 15 KeV.

2.2.3.2 Porosity determination

The porosity of the fabricated scaffold was quantified using Image J software (NIH, USA) from at least 3 different images of both electrospun scaffolds as described earlier (Michalak et al. 2017; Oksa et al. 2011). Porosity calculation using Image J software is the best method, which has been proposed to deliver the reliability of 95% confidence level (Oksa et al. 2011). The procedure to calculate the porosity has been described as flow chart in figure 2.7. The mean threshold method was applied for porosity calculation. The results obtained were plotted using Origin software (Origin Lab Corporation).

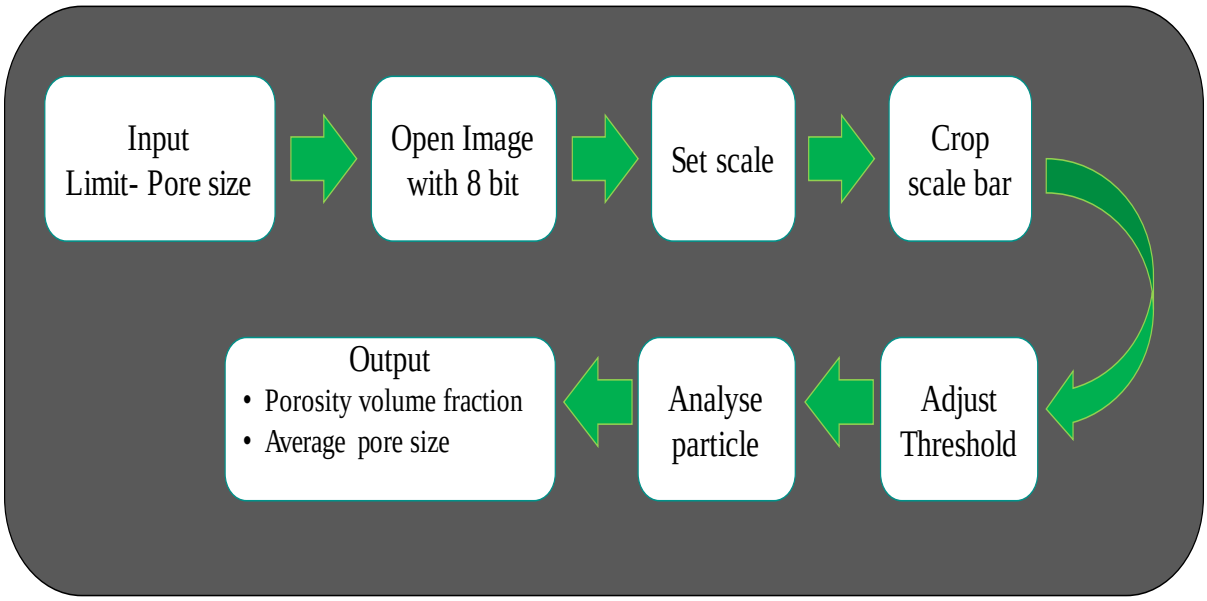

Figure 2.7 Schematic for porosity analysis using Image J software.

2.2.3.3 ATR-FTIR spectroscopic analysis

Infrared spectra for the scaffolds were recorded on Nicolet iS5 THERMO Electron Scientific Instruments LLC equipped with diamond laminate crystal with iD5 attenuated total reflection (ATR) accessory for the scaffolds. 4 cm^{-1} resolutions with 16 scans were taken for all spectra at an infrared range of 500– 4000 cm^{-1}.

2.2.3.4 Water retention capacity

The water retaining capacity of the scaffolds was discerned by soaking the scaffolds in phosphate buffered saline (PBS), pH 7.4 at room temperature for 144 h (i.e., 6 days) (Varshney et al. 2019). Scaffolds used for this study were 10 mm x 10 mm x 0.5 mm (lxbxh). The fluid retention ratio is defined as the ratio of final increased weight to the initial weight. The weight of the wet scaffolds was measured immediately by blotting the surrounding water content with the help of a tissue paper. At least three independent experiments were carried out in triplicates.

The water retention was determined as

$$Swelling\ percentage\ (\%) = \left(\frac{W_{wet} - W_{dry}}{W_{dry}}\right) \times 100 \quad \text{..... (i)}$$

2.2.3.5 In vitro stability and degradation

In vitro stability and biodegradation of the fabricated scaffolds were carried out in a lysozyme solution (10^4 U/mL in distilled water) at 37°C inside a humidified CO_2 incubator. The scaffolds were incubated in the lysozyme solution for 6 days. The lysozyme degradation was observed after 4 h, 10 h, 1 day, 3 day and 6 days of incubation. The scaffolds were weighed at specified

time intervals while maintaining the degrading medium. At the end of the postulated time period the scaffolds degradation percentage was quantified using the following formula-

$$Degradation\ (\%) = \left(\frac{W_i - W_f}{W_i}\right) \times 100 \ldots\ldots\ldots\ldots\ldots\ldots\ldots\ldots\ldots\ldots \text{(ii)}$$

Where W_i and W_f are the initial and final weights of the scaffolds before and after degradation respectively.

2.2.3.6 Transparency determination

Transparency of the scaffolds was measured using a UV-visible spectrophotometer (UV-VIS Spectrophotometer – 2373, Electronics India (EI), India) across the range of visible wavelengths (400-700 nm). The scaffolds were cut into strips with 20 X 9 mm dimensions with a thickness range of 0.5-0.6 mm. The scaffolds were pre-immersed in PBS for 1 h and were loaded in cuvette for transparency measurement. Firstly, the cuvette containing PBS was set as a reference baseline and then the samples were scanned in visible wavelength range (400-700 nm).

2.2.3.7 Cellular viability and compatibility

2.2.3.7.1 Culturing fibroblast cells on the prepared nanofibrous scaffolds

To determine the cellular proliferation and cellular biocompatibility, the silk permeated (SFG) scaffolds (3 mm punched using biopsy punch) were first air dried overnight and soaked in a complete nutrient medium and incubated for 1 h to enrich the scaffolds with nutrients essential for cell growth and proliferation. Tissue culture polystyrene 96-well plates as a two-dimensional (2D) culturing platform were employed as a control for cell culture.

Moreover, scaffolds, as well as control plates, were seeded with 10^4 cells per unit volume. SIRC [Statens Seruminstitut Rabbit Cornea] cells were used for the cytocompatibility

assessment, and the nutrient medium was changed every alternate day. The scaffolds were observed every alternate day for cellular growth and proliferation inside the scaffold.

2.2.3.7.2 MTT assay

Cell proliferation and toxicity were determined by MTT (3-(4, 5-dimethyl-2-thiazolyl)-2,5-diphenyl-2H-tetrazolium bromide, HiMedia) reduction assay using SIRC cells (corneal fibroblast cells). This assay presents a simple colorimetric method for calculating comparative cell viability by using a standard microplate absorbance reader. The MTT test is a colorimetric assay used to measure the metabolic activity of cells. It is based on the ability to reduce the tetrazolium dye MTT to an insoluble, purple-color formazan crystals, which is reliant on the enzymes of nicotinamide adenine dinucleotide phosphate (NADPH) (Figure 2.8). The MTT assay was performed with silk permeated gelatin A composite scaffold placed at the bottom of the 96-well plate following the standard procedure. 3 mm scaffold discs were punched out that were sterilized by exposing them to ultra-violet radiation for 60 minutes inside a biosafety cabinet. Cells cultured in the 2D polystyrene 96-well plates without any scaffolds were taken as a positive control; whereas the cell culture medium alone (without cells) served as the negative control for the experiments. SIRC cells were seeded on each scaffold at a density of $1x10^4$ cells/mL and maintained in a CO_2 incubator (Galaxy® 170 S, Eppendorf, Germany) for 1st day, 3rd day, and 5th day. After incubation, the culture medium was removed from each well and a total of 100 µL solution of medium and MTT (5 mg/mL in PBS) solution was added to each well. After 4 h of incubation with MTT, the formazan crystals formed inside the wells were solubilized using a 100 µL dimethyl sulfoxide (DMSO, HiMedia) solution for 1 h for both control and scaffold samples. The optical absorbance was measured at 570 nm on a

multimode reader (Synergy H1 hybrid, Biotek, USA). Three independent experiments in triplicates were performed for testing the scaffolds.

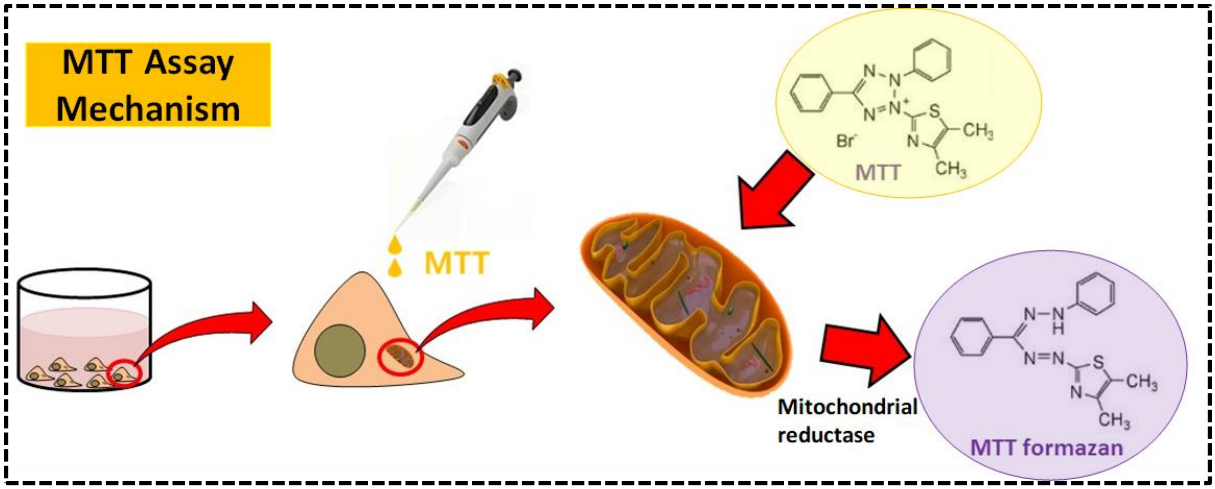

Figure 2.8 Depicts the mechanism of MTT assay to determine the cellular proliferation.

2.2.3.8 Statistical analysis

At least three independent experiments were performed in triplicates, unless otherwise stated and the results were expressed as mean ± standard deviation (SD). One-way analysis of variance (ANOVA) was performed for all the samples followed by Tukey's multiple comparison test to evaluate difference between the groups and considered significant when $p < 0.05$*, $p<0.01$**, $p<0.001$***.

2.3 Results

2.3.1 Morphological characterization

We have studied the scanning electron microscopic (SEM) images of the fabricated scaffolds for their morphological properties. The nanofibers of the fabricated scaffolds were distinctly visible in the obtained micrograph, as shown in figure 2.9. Both types of gelatin scaffolds depict similar nanofibers in a randomly arranged manner. SEM images show good

interconnectivity between the pores of the gelatin A and B nanofibrous mat that would be beneficial for cellular growth and proliferation (Figure 2.9 c and d). The average nanofiber diameter was calculated as 96.09 ± 31.9 nm and 86.07 ± 29.5 nm for gelatin A and B, respectively. Fig.2.10 represents the permeated silk fibroin inside GA nanofibrous scaffold. The scaffolds clearly showed permeation of silk within the nanofibrous pores. SEM images show good interconnectivity between the gelatin A nanofibrous mat pores that would be beneficial for cellular growth and proliferation. Silk occupied the nanofibrous gaps in the silk permeated gelatin (SFG) scaffold, and as a result, the pores in the SFG scaffold are no longer visible through SEM images. The physical crosslinking of silk nanofibers using ethanol vapor provides stability to less stable gelatin nanofibrous scaffolds to withstand the physiological environment and to exhibit optimal cellular growth.

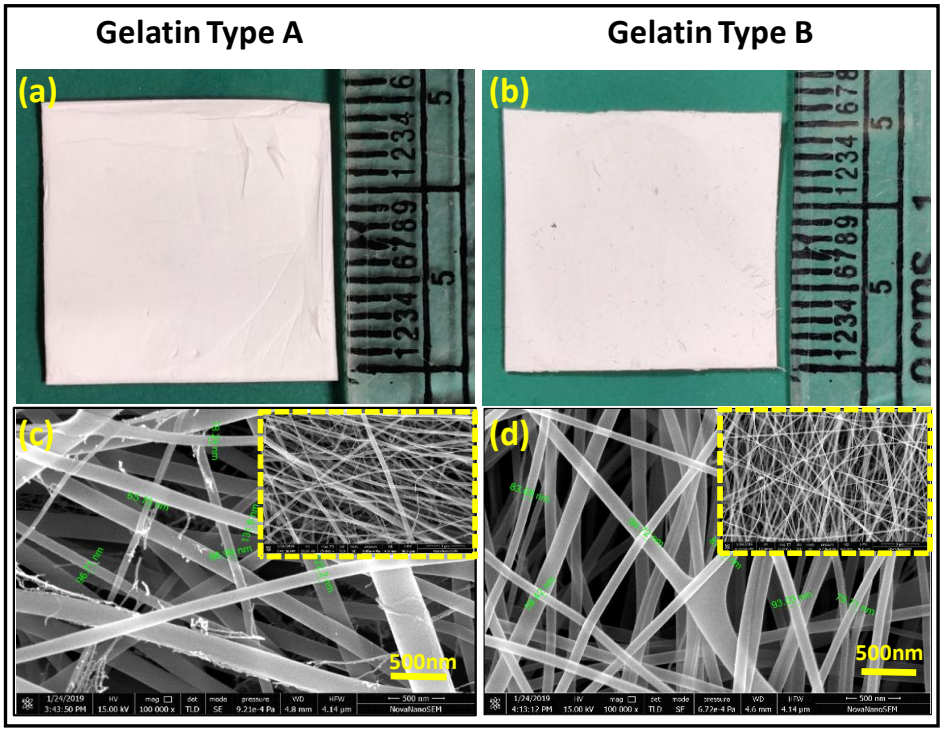

Figure 2.9 Digital images and SEM micrograph of the electrospun gelatin nanofibers. (A) & (B) Digital images and (C) & (D) SEM images of nanofibrous scaffold shows no difference except gelatin B nanofibers appears smooth and thin compared to gelatin type A nanofibers.

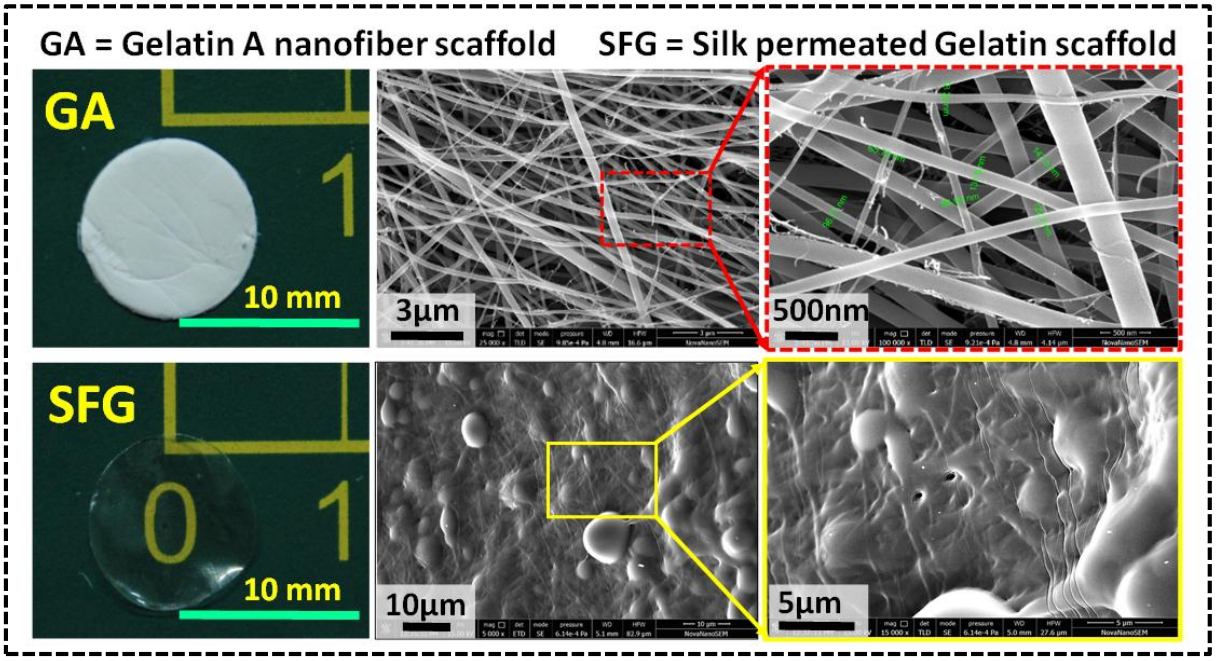

Figure 2.10 Depicts digital images of electrospun gelatin A (GA) and silk permeated nanofibrous gelatin A (SFG), and their respective SEM images.

2.3.2 Porosity determination

The porosity of the prepared scaffolds was measured from the SEM (Scanning electron microscope) images of the gelatin A and B scaffolds using Image J (open, free software for image processing). The threshold method adopted was 'mean'. Porous space between the fibers was found notably high that significantly increased the free space area around the nanofibers. The obtained results showed similar porosity values i.e. 48.08± 3.35 and 51.38 ± 3.72 for gelatin A and gelatin B, respectively (Figure 2.11).

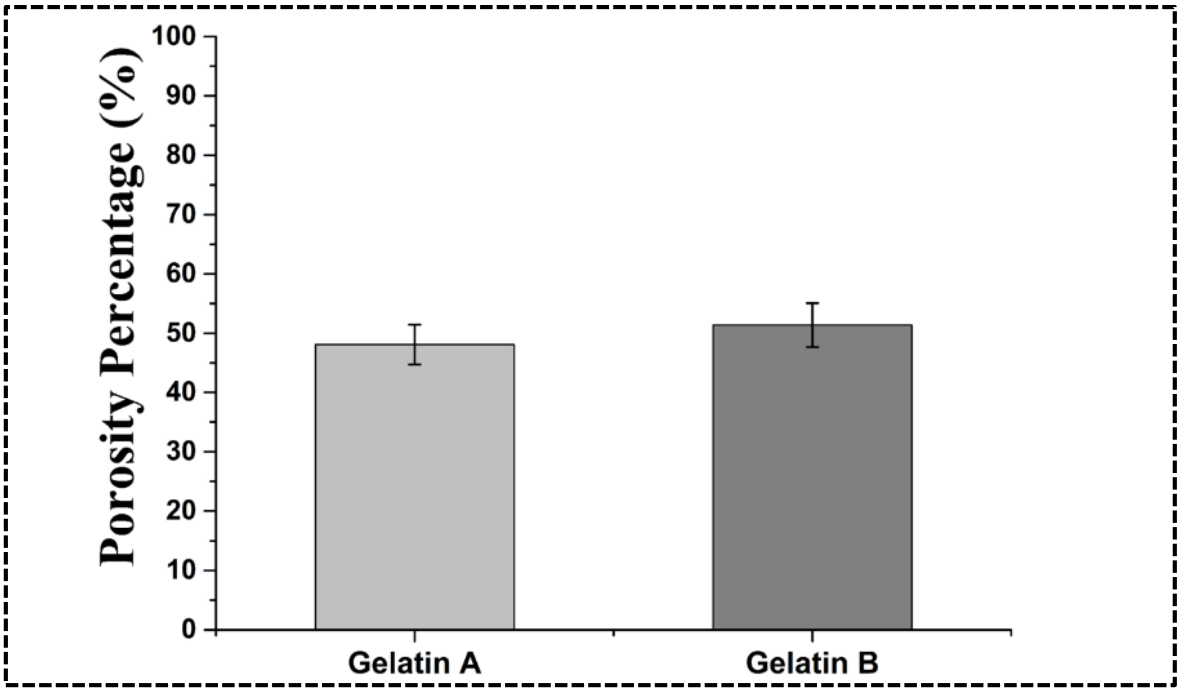

Figure 2.11 Graph represents the porosity percentage obtained using image J software from the scanning electron microscope (SEM) images of the fabricated scaffolds: gelatin A and gelatin B.

2.3.3 ATR-FTIR spectroscopic analysis

Attenuated total reflection-Fourier-transform infrared spectroscopy (ATR-FTIR) of gelatin type A and B nanofibrous sheet was performed to identify the functional groups, probable biomolecules and possible bonds in both the samples. Proteins are a group of amino acids connected by peptide bonds. These polypeptide and proteins repeating units are responsible for IR absorptions bands. These polypeptide and protein repeats give rise to nine characteristic absorption bonds out of which the amide-I represents C=O stretching and could be identified as a peak at 1640 cm^{-1}, N-H bending vibrations and stretching vibrations of C-N were represented by amide-II and display a peak at 1539 cm^{-1}. Amide-III peak is represented at 1240 cm^{-1}, which represents N-H in phase bending and C-N stretching. The peak band 3304 cm^{-1} attributes to hydrogen bond of water and amide A (N-H stretching vibration) (figure 2.12). On

comparing peaks of both the gelatin A and B scaffolds, we observed similar peaks at characteristic wavenumbers with slight change in their peak intensities.

Figure 2.13 shows the various characteristic peaks of gelatin type A nanofibrous sheet, silk nanofibrous scaffold and SFG scaffold; such as, in case of SFG peaks of amide-I represent C=O stretching and could be identified as a peak at 1640 cm^{-1}, N-H in phase bending vibrations and stretching vibrations of C-N were represented by amide-II and display a peak at 1539 cm^{-1}. Amide-III peak is represented at 1240 cm^{-1}, which represent N-H in phase bending and C-N stretching. The peak band 3304 cm^{-1} attributes to hydrogen bond of water and amide A (N-H stretching vibration) (figure 2.13). Moreover, the major peaks for silk film (before ethanol vapor treatment i.e., NT) were detected at 1645, 1530 and 1235 cm^{-1}. These absorption peaks correspond to the peptide backbone of amide I (C=O stretching), amide II (N-H Bending) and amide III (C-N stretching) respectively; representing random coil arrangement of silk I structure. Ethanol vapor treatment of SFG overnight led to shift in the absorption peaks to a slightly lower wavenumber i.e., at 1627 cm^{-1}, 1522 cm^{-1} and 1232 cm^{-1} for amide I, amide II and amide III, respectively; attributing to β sheet formation in silk and furthermore indicating that SFG (after ethanol vapor treatment) mainly exhibited silk II structure (Okhawilai et al. 2010; Amiraliyan, Nouri, and Haghighat Kish 2010; Shen et al. 2015; Yusoff et al. 2019). It is important to note that SFG does not exhibit any alteration in the gelatin peaks after ethanol vapor treatment.

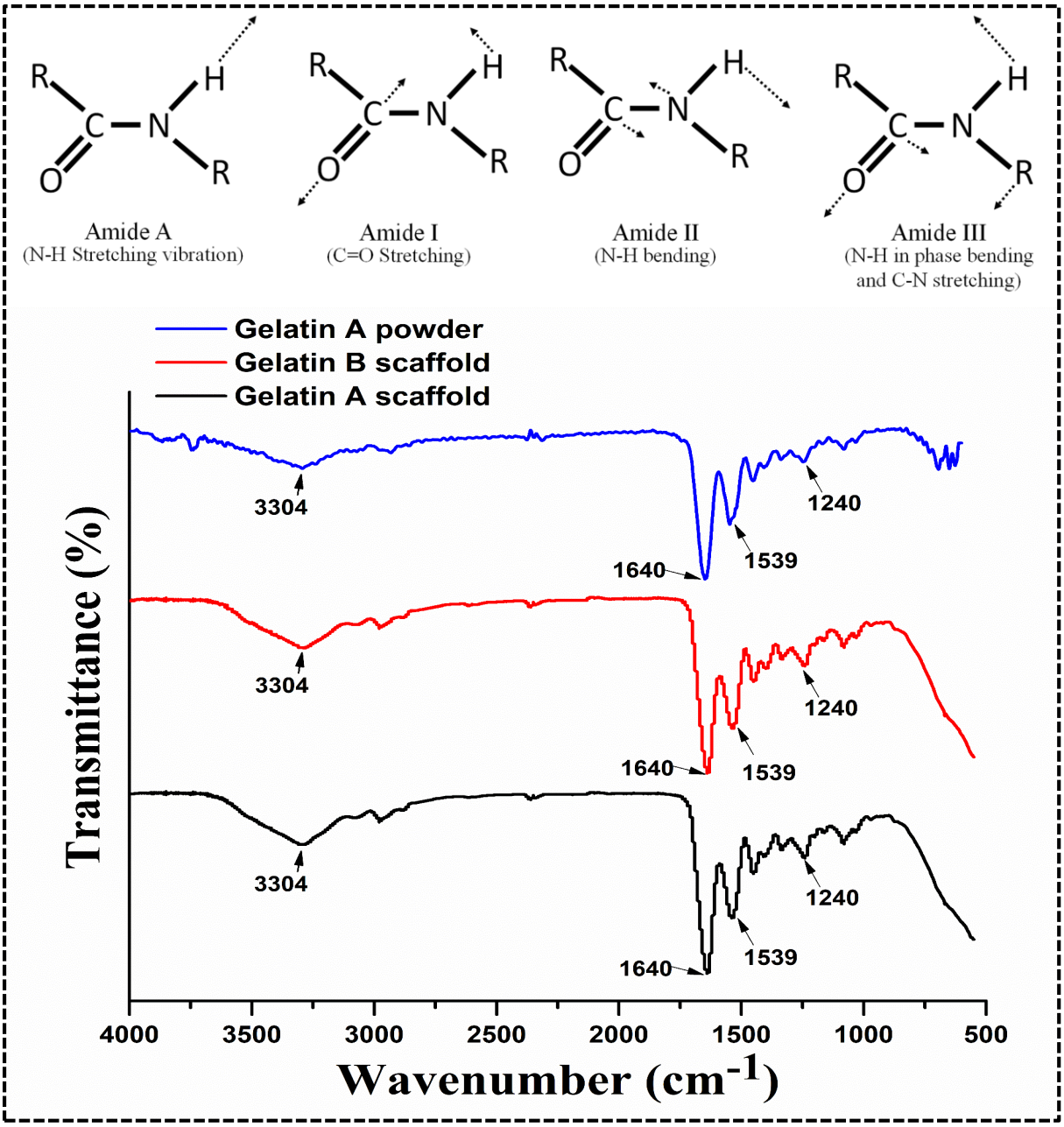

Figure 2.12 Attenuated total Reflection-Fourier-transform infrared spectroscopy (ATR-FTIR) analysis of electrospun gelatin A scaffold, gelatin B scaffold and gelatin A. Both the gelatin A and B polymeric scaffolds show similar characteristic peaks with no significant difference. Gelatin A and gelatin B scaffolds represents characteristic peaks at 1640, 1540, 1455 cm^{-1} and 3304 cm^{-1} for amide I, amide II, amide III and amide A, respectively.

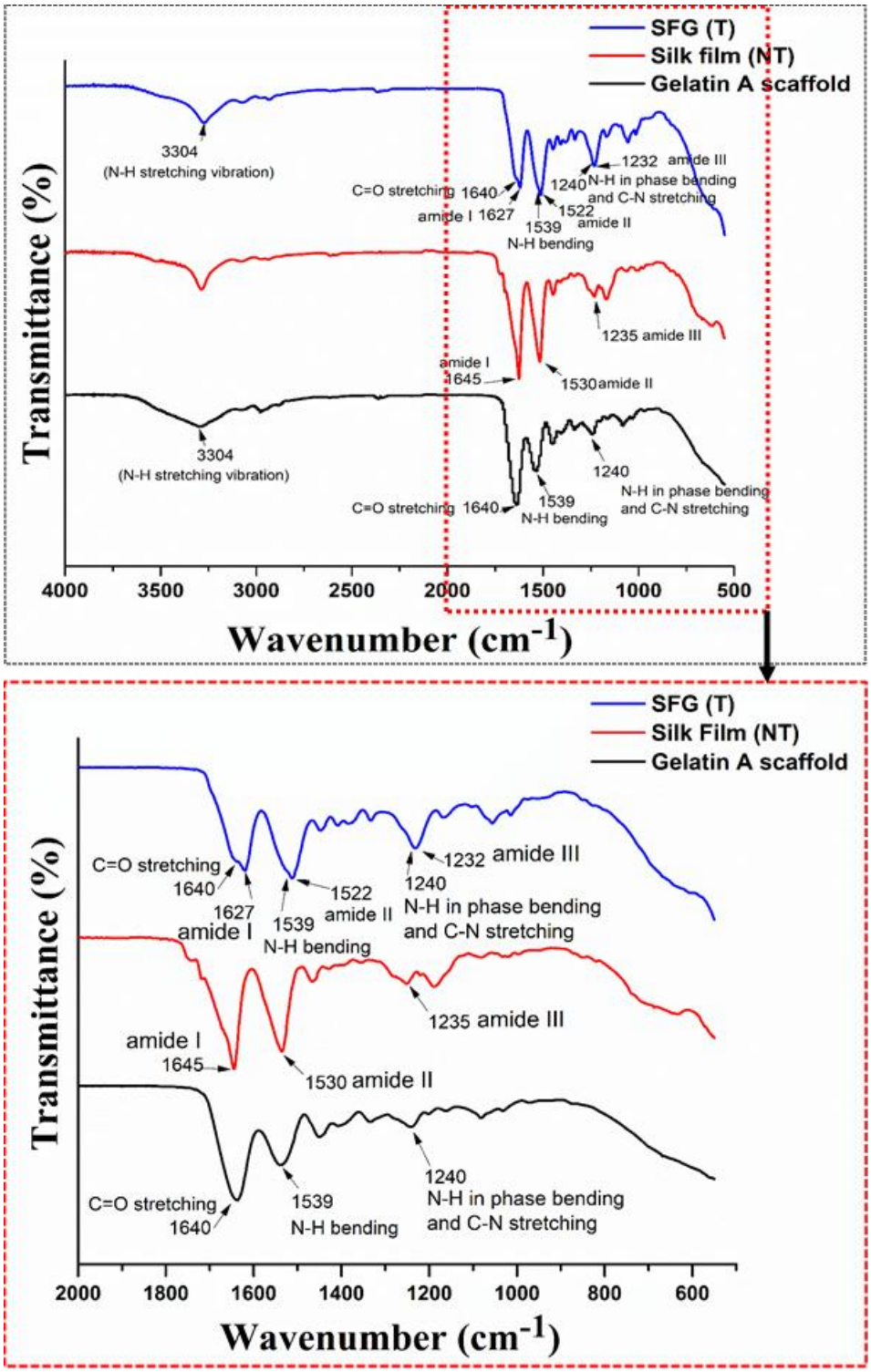

Figure 2.13 Attenuated total reflection-Fourier-transform infrared spectroscopy (ATR-FTIR) analysis of electrospun gelatin A scaffold silk film, and ethanol treated silk permeated gelatin A nanofibrous mat [SFG (T)]. SFG (T) shows all the characteristic peaks of gelatin A and silk,

with a peak shift of silk characteristic peak to a slightly lower wavenumber, i.e., at 1627 cm^{-1}, 1522 $cm^{-1,}$ and 1232 cm^{-1} for amide I, amide II, and amide III, respectively.

2.3.4 Liquid retaining capacity

The results for liquid retaining capacity of the scaffolds are shown in figure 2.14. The dried samples were weighed and then immersed in PBS followed by incubation at room temperature (25^{o}C) as well as at physiological temperature (37^{o}C). Gelatin B scaffold got dissolved quickly in both the conditions, whereas gelatin A gained approximately 800% fluid than its original weight within 2 h and was stable more than 11 h at room temperature. At a physiological temperature (i.e., 37^{o}C), the scaffold gained around 1000% fluid than its dry weight and was stable only up to five hours followed by eventual degradation (figure 2.14). The SFG scaffold after physical crosslinking showed a weight gain up to 960% of the total weight. The SFG scaffold lost a little weight after 5 h after incubation but attained stability after losing little weight. The SFG scaffold was perceived to have enhanced stability i.e., up to 144 h (i.e., 6 days) at physiological temperature. Therefore, the permeation of silk fibroin followed by ethanol treatment led to better stability of the gelatin A nanofibrous scaffold compared to gelatin A (GA) without any treatment.

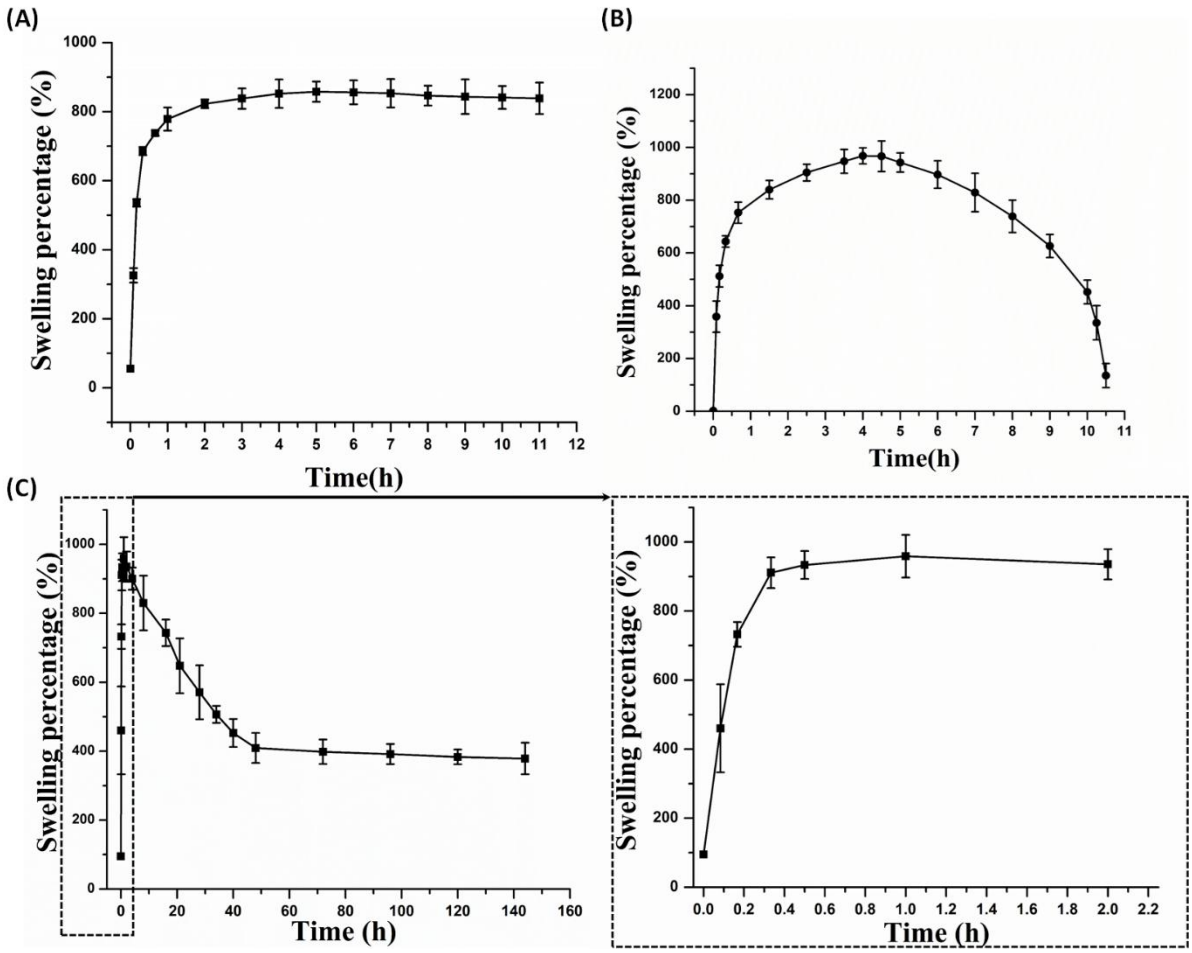

Figure 2.14 Water retention percentage of acid hydrolyzed (gelatin A) scaffold at (A) room temperature (B) at 37°C (physiological temperature) upto 11 h, and (C) electrospun silk permeated gelatin A nanofibrous (SFG) scaffold at 37ºC (physiological temperature) up to 144 h (i.e. 6 days). The gelatin A scaffold incubated at 37°C shows high water holding capacity, but starts degrading after 5 h whereas the samples stored at a room temperature (25°C) remains stable upto 11 h of incubation. Silk permeated electrospun gelatin A nanofibrous scaffold (SFG) remains stable for longer compared to gelatin A alone, providing better opportunity for cellular growth.

2.3.5 Stability and degradation

Stability and degradation of a biomaterial is an essential characteristics of any scaffold to be utilized for tissue engineering application. The evaluation of the stability of fabricated nanofibrous sheet was performed at physiological temperature (37°C). In vitro degradation study in a lysozyme solution was conducted to simulate behavior of nanofibrous scaffold in physiological environment, because of presence of this enzyme in various body fluids including tears and serum (Ren et al. 2005). Digital images of the scaffolds represent the degradation behavior as shown in figure 2.15 (a). The gelatin B degraded quickly within minutes, whereas, gelatin A showed comparatively better stability and almost degraded within 24 h of incubation. The silk permeated gelatin A nanofibrous scaffold (SFG) degraded around 40% of its original weight within 6 days of incubation. Bar graph in figure 2.15 (b) represents the weight loss percentage of gelatin A and SFG nanofibrous scaffolds. Gelatin A nanofibrous scaffolds lost ~35% and ~83% of their initial weight after 4 h and 10 h of incubation, respectively, followed by almost complete degradation 24 h onwards. SFG nanofibrous scaffolds exhibited better stability compared to both gelatin A and B nanofibers. Weight loss percentage for SFG nanofibrous scaffold was found ~6%, ~12%, ~27%, ~32% and ~40% after 4 h, 10 h, 1st day, 3rd day and 6th day of incubation. The small weight loss percentage of SFG scaffold could be attributed to its conversion from hydrophilic and amorphous silk moiety into less hydrophilic and crystalline structure after ethanol treatment. Moreover, gelatin component is likely to be entangled in between crystalline silk structure; facilitating better stability and resistance to lysozyme degradation of SFG scaffold.

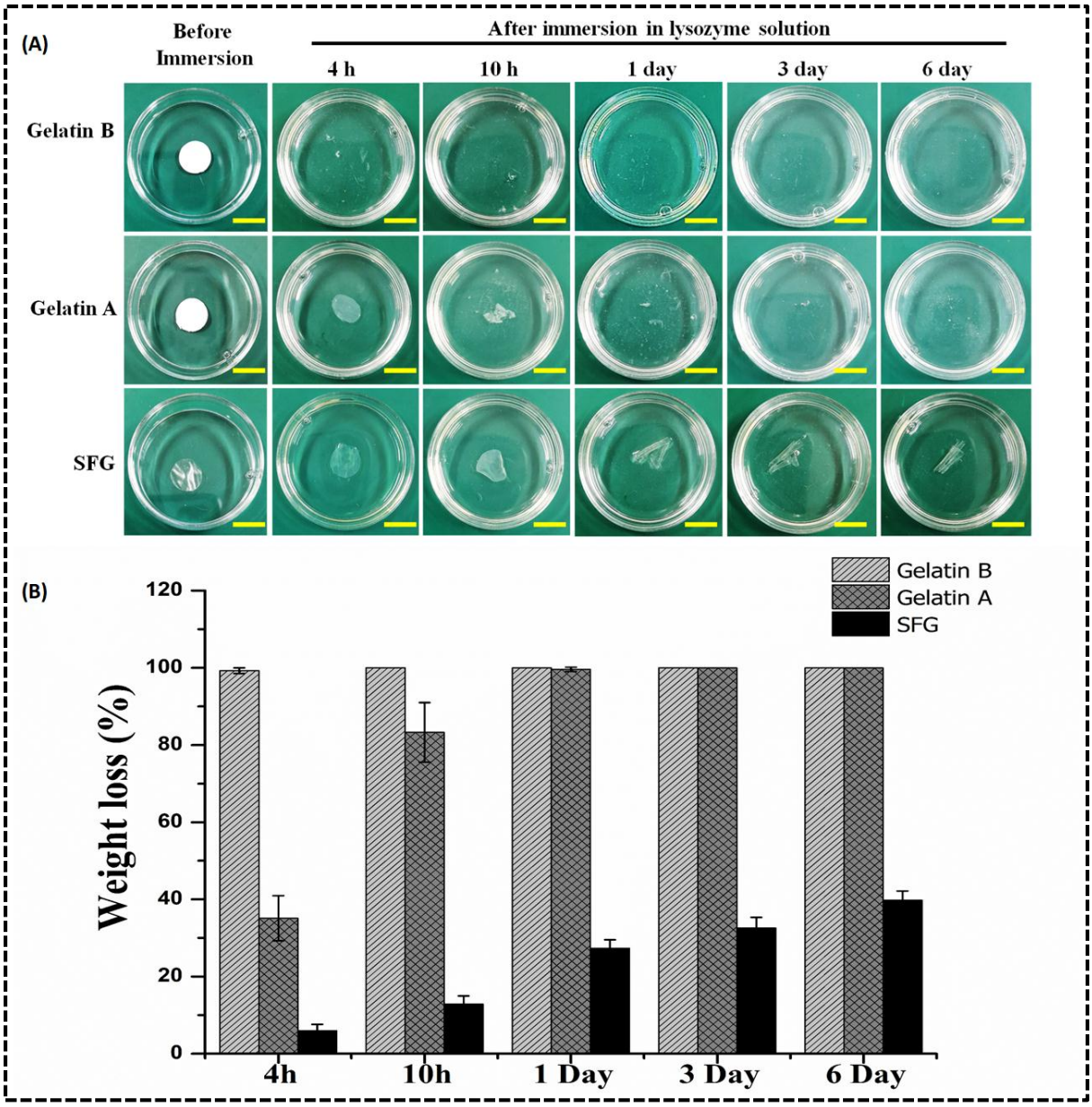

Figure 2.15 Depicts in vitro degradation of scaffolds in lysozyme solution to simulate the in vivo environment of body fluids (A) Digital images of scaffolds showing physical appearance of gelatin A, gelatin B and SFG scaffolds after 4 h, 10 h, 1 day, 3 day and 6 days of incubation in lysozyme solution (B) Represents weight loss percentage of scaffolds after 4 h, 10 h, 1 day, 3 day and 6 days of incubation. Scale bar is 10 mm.

2.3.6 Transparency

The transparency of nanofibrous gelatin B scaffold was not possible to measure as it got dissolved quickly after immersing the scaffold in PBS solution. Gelatin A and SFG scaffolds

were quantified for their transparency. The transparency of nanofibrous gelatin A and SFG scaffolds were further compared with that of adult rat native cornea as shown in figure 2.16. The comparative graph represents the transparency of adult rat cornea (78.38 ± 5.4) similar to acid hydrolyzed gelatin (63.32 ± 5.8), which was found slightly higher than the transparency of silk permeated gelatin A composite scaffold (60.53 ± 10.3) (Table 2.2). Thus, the outcomes revealed the transparency of the scaffolds comparable to that of adult rat cornea, which harbours its tremendous potential to be used for a myriad application in corneal tissue engineering.

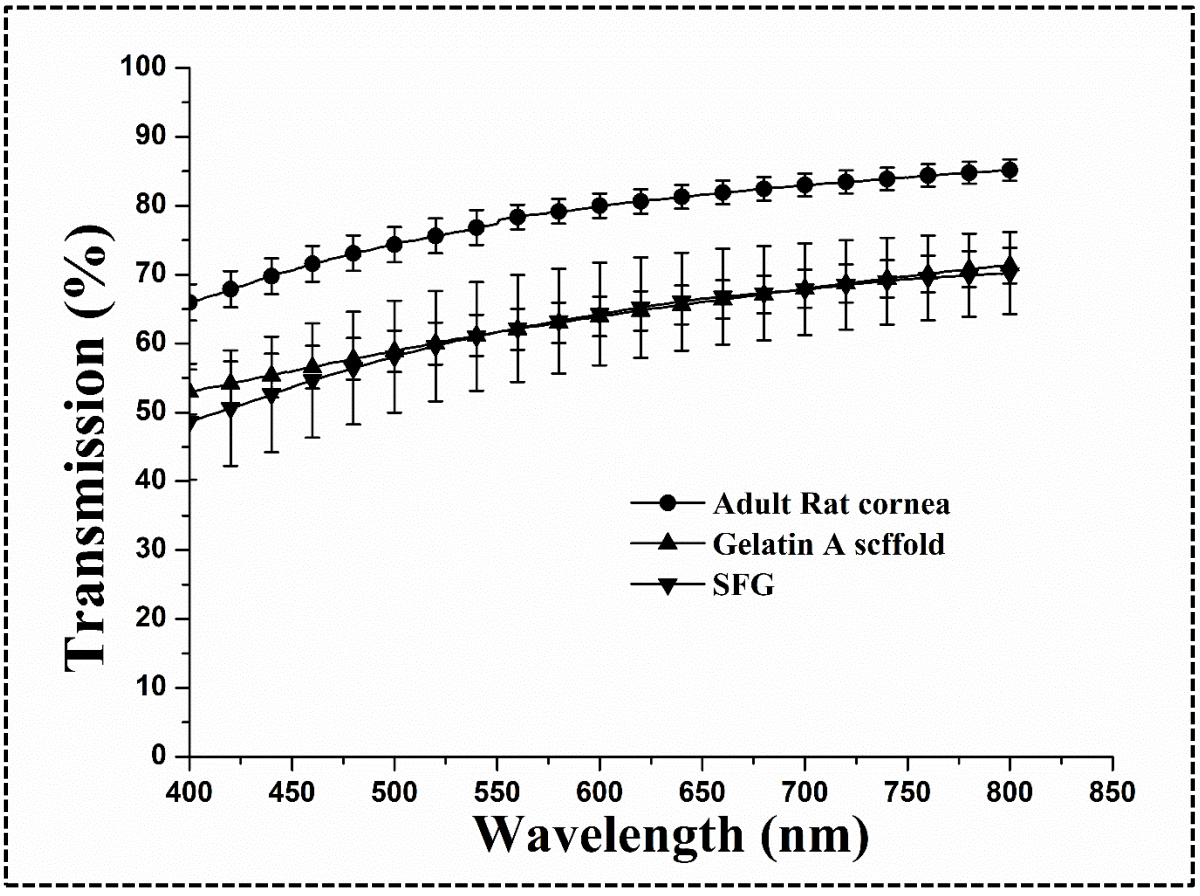

Figure 2.16 Depicts the transparency percentage of the native rat cornea, and fabricated electrospun gelatin type A scaffold and silk permeated gelatin A (SFG) nanofibrous scaffolds. The scaffolds illustrate comparable transparency with respect to native adult rat cornea.

Table 2.2 Transparency percentage of the fabricated scaffolds quantified using UV-Visible spectrophotometer.

S.No.	Scaffold	Transparency (%)
1.	Adult rat cornea	78.38 ± 5.4
2.	Gelatin A scaffold	63.32 ± 5.8
3.	SFG	60.53 ± 10.3

2.3.7 Cellular viability and compatibility

2.3.7.1 Cell culture within the scaffolds

Culturing cells on the prepared scaffold was performed to assess the cytocompatibility of the nanofibrous scaffolds. Gelatin type B scaffold is dissolved immediately when exposed to nutrient medium. As discussed previously, the gelatin A scaffold was found stable up to certain duration at physiological conditions, but start to degrade after 6 h of incubation. Therefore, to maintain stability and observe cell growth and cell compatibility, the concentrated silk fibroin (14-16 % w/v) was permeated inside the gelatin mat, followed by physical crosslinking using 70% ethanol. The obtained results show optimal cell growth and proliferation of fibroblast cells (figure 2.17). Figure 2.17 (a) and (b) represent the bright-field, DAPI stained and merged images of SIRC cell cultured on two-dimensional polystyrene culture plates (TCP) and SFG scaffolds, respectively. The SIRC cells were clearly visible at 10x magnification on the scaffold. Although cells exhibited less expanded shapes on the scaffold, they were showing good proliferation rate as observed from MTT results. No significant compromise in the physical stability and integrity of the scaffolds was perceived in the 96-well polystyrene plate until 6 days of cell culture

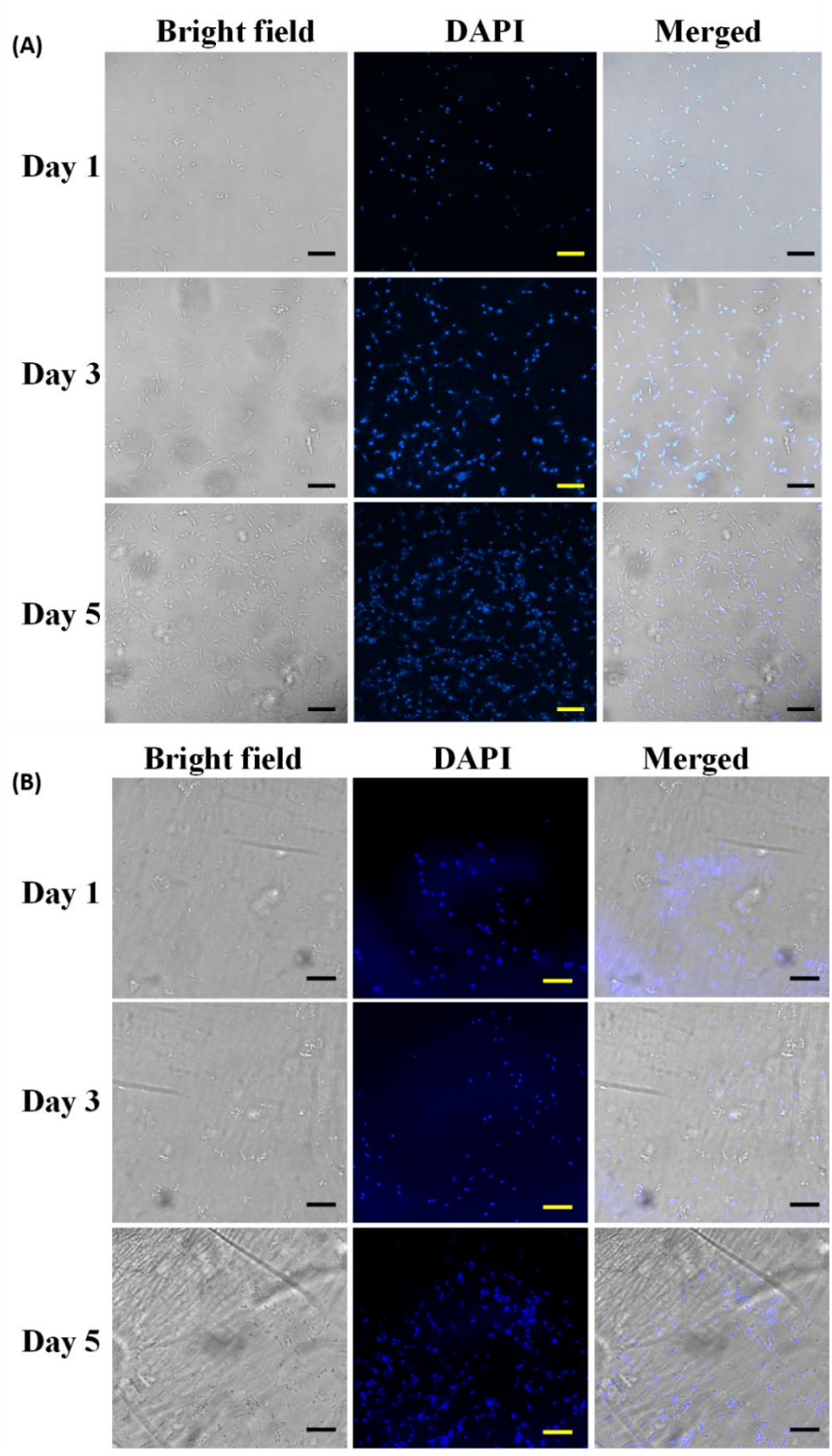

Figure 2.17 Illustrates growth of SIRC [Statens Seruminstitut Rabbit Cornea] fibroblast cells cultured on (A) a culture plate and (B) silk permeated gelatin A (SFG) nanofibrous scaffold for 1, 3, and 5 days. Scale bar is 100 µm.

2.3.7.2 MTT assay

A steady increase in cellular viability was observed over a period of 5 days of culture on the silk permeated, physically crosslinked gelatin A (SFG) scaffold for SIRC cells. The scaffold depicted a consistency in the percentage of cellular proliferation (~ 72%) with respect to 5th day control for SIRC fibroblast cells by 5th day of culture (figure 2.18). Fabricated scaffold assisted growth of fibroblast cells; the proliferation percentage for fibroblast cells was seen to be remarkably optimal by 5th day of cell culture within the scaffolds. Scaffolds showed a noticeable increase in the proliferation percentage of SIRC cells from 21.16 ± 1.73 % on 1st day to 36.18 ± 2.90 % by 3rd day and to 72.46 ± 3.73 % by 5th day with respect to 5th day control for (SIRC) fibroblast cells cultured in 96-well polystyrene plates (figure 2.18).

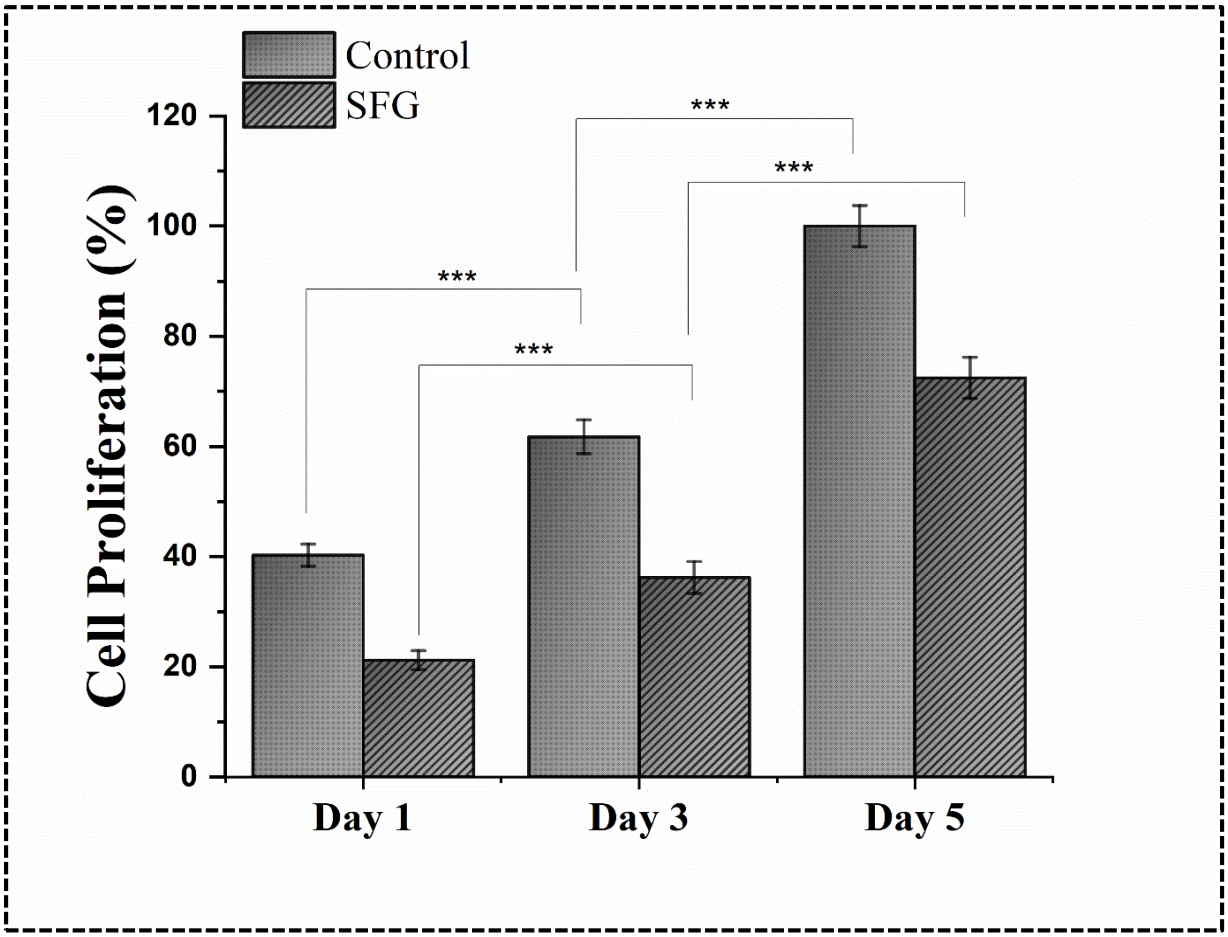

Figure 2.18 This figure illustrates the percentage cellular viability of SIRC [Statens Seruminstitut Rabbit Cornea] fibroblast cells for 1st, 3rd and 5th day of cell culture. Cellular proliferation and compatibility of the electrospun gelatin A permeated nanofibrous (SFG) scaffold determined by MTT assay. In this experiment, absorbance for the 5th day control culture of SIRC cell was considered as reference OD for all the samples. Values are expressed as mean ± SD (n=3) and the level of significance as *p < 0.05 and **p < 0.01, ***p < 0.001, respectively.

2.4 Discussion

Gelatin is the natural polymer that is the most comparable to collagen in terms of chemical characteristics and structural similarity. In compliance with the acid or alkaline/base pre-treatment and thermal denaturation of collagen, gelatin has been divided into two types: acid hydrolyzed gelatin (gelatin A) and base hydrolyzed gelatin (gelatin B). In this study, we have revealed and explained the fabrication and characterization of alkali hydrolyzed and acid hydrolyzed gelatin based electrospun scaffolds that may harbour tremendous applications in corneal tissue engineering. Gelatin A and B represent similar characteristics except a few properties, which have been stated in Table 2.1. Alkali pre-treatment converts amide residue of asparagine and glutamine into aspartic acid and glutamic acid, respectively, leading to relatively more number of carboxylic groups in gelatin B. Among gelatin A and B, the shear modulus (G_e) of gelatin A is expected to be higher because of high bloom strength (300) compared to gelatin B (250). Concentrations of elastic junction (μ) and network chain (ν) are known to affect G_e that determines the polymer network of the gel. At equal degree of swelling, G_e of physical gelatin A gels are found consistently higher than G_e of physical gelatin B gels. Moreover, in a study chemically cross-linked gelatin B gels showed a lower elasticity modulus than chemically cross-linked gelatin A gels wherein the number of chemical junctions was found the same as in the other (Kuijpers et al. 1999b; Lee et al. 2016). This appeared to be in conflict with the fact that gelatin B contains more carboxylic acid groups, which are

available for cross-linking; however, the same is also associated with a higher probability of intramolecular cross-linking, as demonstrated quantitatively by chemical and rheological analysis of the number of cross-links formed (Kuijpers et al. 1999b; Van Vlierberghe et al. 2014). It is known that the chance for intramolecular cross-linking increases upon increasing the number of reactive groups on a polymer chain. Therefore, it is anticipated that the intermolecular interaction between the exposed moieties of gelatin A could be higher compared to that of gelatin B. As a result, gelatin A is expected to demonstrate greater inter-crosslinking for the gelatin A based nanofibrous scaffold, resulting in greater stability as compared to gelatin B nanofibrous scaffolds. From the stability test, we observed that the acid hydrolyzed gelatin electrospun scaffold might serve as a promising candidate for tissue engineering applications in comparison to gelatin B electrospun scaffold. Gelatin A based scaffold maintains its integrity for longer duration at both room temperature as well as at physiological conditions. Although the gelatin A electrospun mat does not perform well at physiological conditions for much longer duration, its transparency feature in an aqueous solvent may enable it to be used in the area of tissue engineering where transparency of the scaffold is an essential requirement (Tonsomboon and Oyen 2013). To overcome the stability issue, various crosslinking agents such as carbodiimides i.e., 1-ethyl-3-(3-dimethylaminopropyl)-1-carbodiimide hydrochloride (EDC) in conjunction with N-hydroxysuccinimide (NHS), glutaraldehyde, genipin, and transglutaminase are used and reported in the literature (Tonsomboon and Oyen 2013; Zhao and Sun 2017; Reddy et al. 2008; Long et al. 2017; Farris, Song, and Huang 2010). These crosslinking agents have been widely exploited to gain optimal mechanical strength and stability, tunable porosity, optimal water imbibing capacity, and extensive porosity in several polymeric biomaterials (Tonsomboon and

Oyen 2013; Zhao and Sun 2017; Reddy et al. 2008; Long et al. 2017). Crosslinkers could be a better alternative to enhance the stability of gelatin based electrospun scaffold. However, they are accompanied with a few limitations such as hampering the transparency, pro-inflammatory effects on macrophage-like cells and causing toxic effect on cellular proliferation (Biscarat et al. 2015; Poursamar et al. 2016).

Ethanol treatment induces crystallinity in the silk fibroin by transforming the secondary structure from random coils to β sheets. Silk fibroin structural protein majorly remains in amorphous state when in liquid form and contains large number of water molecules in between the structure enabling its hydrophilic nature. It undergoes conformational transition among beta sheets, random coil and helices, when exposed to ethanol vapor or methanol or other external stimuli such as water vapor and high intensity UV light (L. Zhang and Webster 2009; Smith and Ma 2004; Buitrago et al. 2018; Hodgkinson, Yuan, and Bayat 2014). The β sheet formation involves the breakage of hydrogen bonds between water and silk and formation of intra/inter-chain hydrogen bonds (Figure 2.6 b) (Lin et al. 2013). Moreover, the obtained FTIR results in figure 2.13 are in agreement with the various studies including the effect of ethanol treatment on the fabricated silk fibroin nanofibers and its composites for tissue engineering applications by Varshney et al. (Varshney et al. 2020), Ning et. al. (Ning et al. 2018) Huang et. al. (Huang et al. 2014) and Zhang et. al. (F. Zhang, Wang, and Zuo 2010). ATR-FTIR of the scaffolds confirms the characteristic peaks of the polymeric materials. SFG reveals the presence of both the polymers i.e., gelatin A and silk. Ethanol vapor treatment shifted major silk characteristic peaks from random coil arrangement (silk I) to beta sheet conformation (silk II), resulting in better stability compared to silk film (NT= non-treated i.e., before ethanol treatment) (Amiraliyan, Nouri, and Haghighat Kish 2010; Shen et al. 2015). The interaction

between the polar groups of silk fibroin chains and ethanol/methanol/water molecules affects the hydrogen bonding between the proteins chains which results in the conversion of less stable, water-soluble amorphous silk into a highly stable, water-insoluble crystalline silk structure (L. Zhang and Webster 2009; Hodgkinson, Yuan, and Bayat 2014; F. Zhang, Wang, and Zuo 2010; Baradaran-Rafii, Biazar, and Heidari-keshel 2016). Silk fibroin protein is a transparent, biocompatible, less degradable and mechanically stable naturally occurring product. These properties of silk entice it as a suitable candidate to be used in combination with gelatin. In our study, we have permeated concentrated silk fibroin (14-16% w/v) within the porous spaces of gelatin A nanofibers followed by physical crosslinking of silk fibroin to enhance the stability of the scaffold. The silk permeated within the pores of nanofibrous gelatin A scaffold increased its stability as well as facilitated adequate time for culturing cells within the scaffold. The electrospinning approach confers high porosity with random/aligned fibrous architecture with high surface to volume ratio and optimal interconnectivity between the nanopores within the nanofibrous structures (Mohammadzadehmoghadam and Dong 2019; Singh, Bandyopadhyay, and Mandal 2019). Porosity in between the electrospun nanofibers plays an essential role to interconnect cellular interaction as well as proper nutrient distribution to each and every cell inside the scaffold (Mohammadzadehmoghadam and Dong 2019). The SEM images of the scaffolds confirm the random nanofibrous structure and its high porosity has been elucidated using ImageJ software. The electrospun nanofibrous scaffolds hold an advantage of enhanced mechanical property that has been extensively discussed in the literatures (Tonsomboon and Oyen 2013; 2013; Hwang et al. 2016; Poddar et al. 2019). Moreover, this unique feature provides more cellular growth and proliferation (Balavigneswaran et al. 2018; Poddar et al. 2019).

Crosslinking or blending the scaffold with the silk fibroin enhances its characteristics including stability and cellular proliferation, which renders them a potent biomaterial for tissue engineering and drug delivery applications. Gelatin enhances the hydrophilicity of the scaffold that permits cellular biocompatibility and supports viability with controlled degradation (Alihosseini 2016; Salvatore et al. 2012). Reported corneal transparency of various organisms varies based on the thickness of the cornea. The transparency is measured in the visible range and maximum transparency is quantified at a wavelength of~800 nm. The human native cornea shows a transparency in a range of 70-90%, which is comparable to the native cornea of porcine and goat (Chakraborty et al. 2019; Choi et al. 2010; Meek and Knupp 2015; Murab, Chameettachal, and Ghosh 2016; Nara et al. 2016; Shi et al. 2019; Tonsomboon and Oyen 2013). The comparative study of visible light transparency percentage depicts that silk permeated gelatin type A scaffold shows the transparency close to those of the native rat cornea (Chakraborty et al. 2019; 2019; Choi et al. 2010; Maurice 1957; Meek and Knupp 2015; Murab, Chameettachal, and Ghosh 2016; Shi et al. 2019). Figure 2.16 depicts the transparency of fabricated nanofibrous scaffold comparable to adult rat cornea as physiological basis of reference. There are a few studies that reveal transparency value and/or spectrum of transparency levels that seem to be similar to that of an adult rat cornea. e.g. Zhang et al., have shown maximum transparency of rat cornea around 70% at a wavelength of 700 nm and minimum transparency of rat cornea around 45% at wavelength 450 nm. However, we have obtained slightly higher transparency level with a similar spectral trend (maximum transparency ~78% at a wavelength of 700 nm and minimum transparency of rat cornea around 68% at a wavelength 450 nm). The maximum transparency of fabricated nanofibrous scaffold (SFG) is obtained ~60% at a wavelength of 700 nm and minimum transparency around 50%

at a wavelength 450 nm). However, the thickness of the construct we have used in the study is around ~400-500 μm, which is analogous to the thickness of the human cornea; in contrast, the thickness of adult rat cornea thickness is reported to be approximately 126.89 ± 11.11 μm (Schulz et al. 2003). Furthermore, it is generally known that 'path length' is a critical component in determining absorbance/transmittance, as demonstrated by Beer–Lambert law (Kocsis, Herman, and Eke 2006). Therefore, it is expected that the fabricated nanofibrous scaffold when trimmed down to the thickness of adult rat cornea would deliver comparable transparency. Cellular compatibility of the scaffold was supported by the viability percentages obtained from MTT assay. Cell proliferation study supports the fact that the obtained electrospun gelatin A scaffold was highly compatible for corneal fibroblast cells which was in agreement with the microscopic observations. Although there are a few reports that proposed electrospun gelatin, collagen and other polymers based scaffolds for corneal tissue engineering applications (Hazra et al. 2016; Kong and Mi 2016; Lawrence et al. 2009; Mohammadzadehmoghadam and Dong 2019; Tonsomboon and Oyen 2013; Wu et al. 2018), our developed silk permeated electrospun gelatin based scaffold to the best of our knowledge appear to be a novel biomaterial possessing the major properties of native human cornea. Such a set of properties confers the efficacy of the electrospun gelatin based implants for cornea and other relevant areas of tissue engineering.

2.5 Conclusion

The present work demonstrates the comparative study of acid hydrolyzed against alkali-hydrolyzed electrospun gelatin scaffolds, which are the potent polymeric biomaterial for tissue engineering. Both gelatin A and gelatin B have been widely used in scaffold fabrication, commercial products, sustained released drug delivery; however, to the best of our knowledge,

we are the first one to reveal a comparative study between nanofibrous scaffolds of gelatin A and gelatin B, fabricated using ternary solvent (glacial acetic acid/ ethyl acetate/water). Electrospinning techniques add-up high surface-to-volume ratio and high porosity to the scaffolds prepared using gelatin. Both gelatin nanofibrous scaffolds shows randomly organized nanofibers with excellent interconnectivity between pores, which is advantageous for cellular growth and proliferation. The gelatin A based electrospun scaffold shows water holding capacity around 800%, with optimal stability at a room temperature, enabling it as a promising candidate for various drug delivery, hydrogel and tissue engineering applications. Gelatin type A nanofibrous sheet without crosslinking is unable to withstand physiological conditions solely. Therefore, silk permeation followed by physical crosslinking substantially improves the stability of the gelatin scaffold. GA scaffold and silk permeated gelatin A nanofibrous scaffold (SFG) showed 50-70% of transparency comparable to that of adult rat cornea. ATR-FTIR analysis showed the presence of their native functional groups and bonds. GA scaffold remained stable up to ~ 11 h at 25˚C, however was found degraded within 24 h when incubated at 37˚C. Furthermore, SFG scaffolds physically cross-linked with ethanol vapor displayed relatively improved stability when examined for at least 6 days at 37°C, minor weight loss when incubated in a lysozyme solution and facilitated significant liquid retention capacity i.e., ~ 960%. The nanofibrous gelatin A scaffold permeated with silk fibroin provides optimal stability as well as proliferation of corneal fibroblast cells close to 72% compared to that of the 5^{th} day control. The degradation rate and stability could further be tuned using chemical or enzymatic cross linkers depending upon the requirements. Thus, the outcomes reveal that the electrospun gelatin A permeated with silk scaffold possesses relatively more stability and therefore could be potentially useful for corneal tissue

engineering and regenerative medicine applications. To the best of our knowledge, our fabricated silk permeated electrospun gelatin-based scaffold appears to be a new biomaterial with the primary characteristics of native human cornea. This combination of characteristics contributes to the efficacy of electrospun gelatin-based implants for corneal and other tissue engineering applications.

2.6 References

Alihosseini, F. 2016. "10 - Plant-Based Compounds for Antimicrobial Textiles." In *Antimicrobial Textiles*, edited by Gang Sun, 155–95. Woodhead Publishing Series in Textiles. Woodhead Publishing. https://doi.org/10.1016/B978-0-08-100576-7.00010-9.

Amiraliyan, N., M. Nouri, and M. Haghighat Kish. 2010. "Structural Characterization and Mechanical Properties of Electrospun Silk Fibroin Nanofiber Mats." *Polymer Science Series A* 52 (4): 407–12. https://doi.org/10.1134/S0965545X10040097.

Aramwit, Pornanong, Nungruthai Jaichawa, Juthamas Ratanavaraporn, and Teerapol Srichana. 2015. "A Comparative Study of Type A and Type B Gelatin Nanoparticles as the Controlled Release Carriers for Different Model Compounds." *Materials Express* 5 (3): 241–48. https://doi.org/10.1166/mex.2015.1233.

Aziz, Soroush, Mohammad Sabzi, Ali Fattahi, and Elham Arkan. 2017. "Electrospun Silk Fibroin/PAN Double-Layer Nanofibrous Membranes Containing Polyaniline/TiO2 Nanoparticles for Anionic Dye Removal." *Journal of Polymer Research* 24 (9): 140. https://doi.org/10.1007/s10965-017-1298-0.

Balavigneswaran, Chelladurai Karthikeyan, Sanjeev Kumar Mahto, Arun Kumar Mahanta, Rajshree Singh, Mahalingam Rajamanickam Vijayakumar, Biswajit Ray, and Nira

Misra. 2018. “Cell Proliferation Influenced by Matrix Compliance of Gelatin Grafted Poly(d,l-Lactide) Three Dimensional Scaffolds.” *Colloids and Surfaces B: Biointerfaces* 166 (June): 170–78. https://doi.org/10.1016/j.colsurfb.2018.03.014.

Bandyk, Dennis F., Michael L. Novotney, Brad L. Johnson, Martin R. Back, and Steven R. Roth. 2001. “Use of Rifampin-Soaked Gelatin-Sealed Polyester Grafts for in Situ Treatment of Primary Aortic and Vascular Prosthetic Infections.” *Journal of Surgical Research* 95 (1): 44–49. https://doi.org/10.1006/jsre.2000.6035.

Baradaran-Rafii, Alireza, Esmaeil Biazar, and Saeed Heidari-keshel. 2016. “Cellular Response of Limbal Stem Cells on Polycaprolactone Nanofibrous Scaffolds for Ocular Epithelial Regeneration.” *Current Eye Research* 41 (3): 326–33. https://doi.org/10.3109/02713683.2015.1019004.

Barchuk, Mykhailo, Pavla Čapková, Zdeňka Kolská, Jindřich Matoušek, David Poustka, Lucie Šplíchalová, Oldřich Benada, and Marcela Munzarová. 2016. “Structure and Surface Properties of Chitosan/PEO/Gelatin Nanofibrous Membrane.” *Journal of Polymer Research* 23 (2): 20. https://doi.org/10.1007/s10965-015-0906-0.

Biscarat, Jennifer, Benjamin Galea, José Sanchez, and Celine Pochat-Bohatier. 2015. “Effect of Chemical Cross-Linking on Gelatin Membrane Solubility with a Non-Toxic and Non-Volatile Agent: Terephthalaldehyde.” *International Journal of Biological Macromolecules* 74 (March): 5–11. https://doi.org/10.1016/j.ijbiomac.2014.11.022.

Buitrago, Jennifer O., Kapil D. Patel, Ahmed El-Fiqi, Jung-Hwan Lee, Banani Kundu, Hae-Hyoung Lee, and Hae-Won Kim. 2018. “Silk Fibroin/Collagen Protein Hybrid Cell-Encapsulating Hydrogels with Tunable Gelation and Improved Physical and Biological Properties.” *Acta Biomaterialia* 69: 218–33.

https://doi.org/10.1016/j.actbio.2017.12.026.

Chakraborty, Juhi, Subhadeep Roy, Sumit Murab, Raghav Ravani, Kulwinder Kaur, Saranya Devi, Divya Singh, et al. 2019. "Modulation of Macrophage Phenotype, Maturation, and Graft Integration through Chondroitin Sulfate Cross-Linking to Decellularized Cornea." *ACS Biomaterials Science & Engineering* 5 (1): 165–79. https://doi.org/10.1021/acsbiomaterials.8b00251.

Chen, Shaoyong, Mingyue Liu, Huiming Huang, Lan Cheng, and Hong-Ping Zhao. 2019. "Mechanical Properties of Bombyx Mori Silkworm Silk Fibre and Its Corresponding Silk Fibroin Filament: A Comparative Study." *Materials & Design* 181 (November): 108077. https://doi.org/10.1016/j.matdes.2019.108077.

Choi, Jin San, James K. Williams, Margaret Greven, Keith A. Walter, Patrick W. Laber, Gilson Khang, and Shay Soker. 2010. "Bioengineering Endothelialized Neo-Corneas Using Donor-Derived Corneal Endothelial Cells and Decellularized Corneal Stroma." *Biomaterials* 31 (26): 6738–45. https://doi.org/10.1016/j.biomaterials.2010.05.020.

Choktaweesap, Nuanchan, Kunawan Arayanarakul, Duangdao Aht-ong, Chidchanok Meechaisue, and Pitt Supaphol. 2007. "Electrospun Gelatin Fibers: Effect of Solvent System on Morphology and Fiber Diameters." *Polymer Journal* 39 (6): 622–31. https://doi.org/10.1295/polymj.PJ2006190.

Dadras Chomachayi, Masoud, Atefeh Solouk, Somaye Akbari, Davoud Sadeghi, Fereshteh Mirahmadi, and Hamid Mirzadeh. 2018. "Electrospun Nanofibers Comprising of Silk Fibroin/Gelatin for Drug Delivery Applications: Thyme Essential Oil and Doxycycline Monohydrate Release Study: Electrospun Silk/Gelatin Nanofibers." *Journal of*

Biomedical Materials Research Part A 106 (4): 1092–1103. https://doi.org/10.1002/jbm.a.36303.

Deshmukh, K., M. Basheer Ahamed, R. R. Deshmukh, S. K. Khadheer Pasha, P. R. Bhagat, and K. Chidambaram. 2017. "3 - Biopolymer Composites With High Dielectric Performance: Interface Engineering." In *Biopolymer Composites in Electronics*, edited by K. K. Sadasivuni, D. Ponnamma, J. Kim, J. -J. Cabibihan, and M. A. AlMaadeed, 27–128. Elsevier. https://doi.org/10.1016/B978-0-12-809261-3.00003-6.

Djagny, V. B., Z. Wang, and S. Xu. 2001. "Gelatin: A Valuable Protein for Food and Pharmaceutical Industries: Review." *Critical Reviews in Food Science and Nutrition* 41 (6): 481–92. https://doi.org/10.1080/20014091091904.

Faradiella, Hanandyta, Putri Dewi Fatwa Ningsih, and Warlinda Eka Triastuti. 2017. "The Acid Solvent Experimental Studies on Gelatin Producing by Utilizing Snapper Fishes Scales Waste (Lutjanus Camphecanus Sp.)." In , 020042. Las Vegas, Nevada, USA. https://doi.org/10.1063/1.4978115.

Farasatkia, Asal, Mahshid Kharaziha, Fakhreddin Ashrafizadeh, and Sahar Salehi. 2021. "Transparent Silk/Gelatin Methacrylate (GelMA) Fibrillar Film for Corneal Regeneration." *Materials Science and Engineering: C* 120 (January): 111744. https://doi.org/10.1016/j.msec.2020.111744.

Farris, Stefano, Jianhui Song, and Qingrong Huang. 2010. "Alternative Reaction Mechanism for the Cross-Linking of Gelatin with Glutaraldehyde." *Journal of Agricultural and Food Chemistry* 58 (2): 998–1003. https://doi.org/10.1021/jf9031603.

Foox, Maytal, and Meital Zilberman. 2015. “Drug Delivery from Gelatin-Based Systems.” *Expert Opinion on Drug Delivery* 12 (9): 1547–63. https://doi.org/10.1517/17425247.2015.1037272.

Guidetti, Giulia, Yu Wang, and Fiorenzo G. Omenetto. 2020. “Active Optics with Silk: Silk Structural Changes as Enablers of Active Optical Devices.” *Nanophotonics* 1 (ahead-of-print). https://doi.org/10.1515/nanoph-2020-0358.

Hajikarimi, Amir, and Mohammad Sadeghi. 2020. “Free Radical Synthesis of Cross-Linking Gelatin Base Poly NVP/Acrylic Acid Hydrogel and Nanoclay Hydrogel as Cephalexin Drug Deliver.” *Journal of Polymer Research* 27 (3): 57. https://doi.org/10.1007/s10965-020-2020-1.

Hazra, Sarbani, Sudip Nandi, Deboki Naskar, Rajdeep Guha, Sushovan Chowdhury, Nirparaj Pradhan, Subhas C. Kundu, and Aditya Konar. 2016. “Non-Mulberry Silk Fibroin Biomaterial for Corneal Regeneration.” *Scientific Reports* 6 (February). https://doi.org/10.1038/srep21840.

Hodgkinson, Tom, Xue-Feng Yuan, and Ardeshir Bayat. 2014. “Electrospun Silk Fibroin Fiber Diameter Influences in Vitro Dermal Fibroblast Behavior and Promotes Healing of Ex Vivo Wound Models.” *Journal of Tissue Engineering* 5 (February): 204173141455166. https://doi.org/10.1177/2041731414551661.

Huang, Xiangyu, Suna Fan, Alhadi Ibrahim Mohammed Altayp, Yaopeng Zhang, Huili Shao, Xuechao Hu, Minkai Xie, and Yuemin Xu. 2014. “Tunable Structures and Properties of Electrospun Regenerated Silk Fibroin Mats Annealed in Water Vapor at Different Times and Temperatures.” Research Article. Journal of Nanomaterials. Hindawi. May 5, 2014. https://doi.org/10.1155/2014/682563.

Huda, Muhsina K., Pranjal P. Das, Shashi D. Baruah, and Prakash J. Saikia. 2017. "Polycaprolactone-Blended Gelatin Microspheres and Their Morphological Study." *Journal of Polymer Research* 24 (5): 72. https://doi.org/10.1007/s10965-017-1229-0.

Hussein, Kamal H., Kyung-Mee Park, Yun-Suk Lee, Jae-Seok Woo, Byung-Jae Kang, Ki-Young Choi, Kyung-Sun Kang, and Heung-Myong Woo. 2017. "New Insights into the Pros and Cons of Cross-Linking Decellularized Bioartificial Organs." *The International Journal of Artificial Organs* 40 (4): 136–41. https://doi.org/10.5301/ojao.5000541.

Hwang, Patrick T.J., Kyle Murdock, Grant C. Alexander, Amanee D. Salaam, Joshua I. Ng, Dong-Jin Lim, Derrick Dean, and Ho-Wook Jun. 2016. "Poly(ε-Caprolactone)/Gelatin Composite Electrospun Scaffolds with Porous Crater-like Structures for Tissue Engineering." *Journal of Biomedical Materials Research. Part A* 104 (4): 1017–29. https://doi.org/10.1002/jbm.a.35614.

Jang, Hyun-Jun, Yu-Mi Kim, Bo-Young Yoo, and Young-Kwon Seo. 2018. "Wound-Healing Effects of Human Dermal Components with Gelatin Dressing." *Journal of Biomaterials Applications* 32 (6): 716–24. https://doi.org/10.1177/0885328217741758.

Ji, Lijun, Mindong Gong, Wei Qiao, Wenqian Zhang, Qingren Liu, Richard Erick Dunham, and Jun Gu. 2018. "A Gelatin/PLA-b-PEG Film of Excellent Gas Barrier and Mechanical Properties." *Journal of Polymer Research* 25 (10): 210. https://doi.org/10.1007/s10965-018-1600-9.

Kocsis, L., P. Herman, and A. Eke. 2006. "The Modified Beer–Lambert Law Revisited." *Physics in Medicine and Biology* 51 (5): N91–98. https://doi.org/10.1088/0031-9155/51/5/N02.

Kommareddy, Sushma, Dinesh Shenoy, and Mansoor Amiji. 2007. "Gelatin Nanoparticles and Their Biofunctionalization." In *Nanotechnologies for the Life Sciences, Vol. 1 Biofunctionalization of Nanomaterials*. https://doi.org/10.1002/9783527610419.ntls0011.

Kong, Bin, and Shengli Mi. 2016. "Electrospun Scaffolds for Corneal Tissue Engineering: A Review." *Materials* 9 (8). https://doi.org/10.3390/ma9080614.

Kshitiz, JinSeok Park, Peter Kim, Wilda Helen, Adam J. Engler, Andre Levchenko, and Deok-Ho Kim. 2012. "Control of Stem Cell Fate and Function by Engineering Physical Microenvironments." *Integrative Biology* 4 (9): 1008–18. https://doi.org/10.1039/C2IB20080E.

Kuijpers, A. J., G. H. M. Engbers, J. Feijen, S. C. De Smedt, T. K. L. Meyvis, J. Demeester, J. Krijgsveld, S. A. J. Zaat, and J. Dankert. 1999a. "Characterization of the Network Structure of Carbodiimide Cross-Linked Gelatin Gels." *Macromolecules* 32 (10): 3325–33. https://doi.org/10.1021/ma981929v.

Kujala, S., Anna Mannila, L. Karvonen, K. Kieu, and Z. Sun. 2016. "Natural Silk as a Photonics Component: A Study on Its Light Guiding and Nonlinear Optical Properties." *Scientific Reports*. https://doi.org/10.1038/srep22358.

Land, Michael H., Mark D. Piehl, and A. Wesley Burks. 2013. "Near Fatal Anaphylaxis from Orally Administered Gelatin Capsule." *The Journal of Allergy and Clinical Immunology: In Practice* 1 (1): 99–100. https://doi.org/10.1016/j.jaip.2012.09.004.

Lawrence, Brian D., Mark Cronin-Golomb, Irene Georgakoudi, David L. Kaplan, and Fiorenzo G. Omenetto. 2008. “Bioactive Silk Protein Biomaterial Systems for Optical Devices.” *Biomacromolecules* 9 (4): 1214–20. https://doi.org/10.1021/bm701235f.

Lawrence, Brian D., Jeffrey K. Marchant, Mariya A. Pindrus, Fiorenzo G. Omenetto, and David L. Kaplan. 2009. “Silk Film Biomaterials for Cornea Tissue Engineering.” *Biomaterials* 30 (7): 1299–1308. https://doi.org/10.1016/j.biomaterials.2008.11.018.

Lee, Bae Hoon, Nathaniel Lum, Li Yuan Seow, Pei Qi Lim, and Lay Poh Tan. 2016. “Synthesis and Characterization of Types A and B Gelatin Methacryloyl for Bioink Applications.” *Materials* 9 (10). https://doi.org/10.3390/ma9100797.

Li, Qingsong, Ning Qi, Yu Peng, Yafeng Zhang, Lei Shi, Xiaohua Zhang, Yuekun Lai, Kai Wei, Ick Soo Kim, and Ke-Qin Zhang. 2017. “Sub-Micron Silk Fibroin Film with High Humidity Sensibility through Color Changing.” *RSC Advances* 7 (29): 17889–97. https://doi.org/10.1039/C6RA28460D.

Lin, Yinan, Xiaoxia Xia, Ke Shang, Roberto Elia, Wenwen Huang, Peggy Cebe, Gary Leisk, Fiorenzo Omenetto, and David L. Kaplan. 2013. “Tuning Chemical and Physical Cross-Links in Silk Electrogels for Morphological Analysis and Mechanical Reinforcement.” *Biomacromolecules* 14 (8): 2629–35. https://doi.org/10.1021/bm4004892.

Long, Haiyan, Kunlong Ma, Zhenghua Xiao, Xiaomei Ren, and Gang Yang. 2017. “Preparation and Characteristics of Gelatin Sponges Crosslinked by Microbial Transglutaminase.” *PeerJ* 5 (August). https://doi.org/10.7717/peerj.3665.

Massoumi, Bakhshali, Reza Massoumi, Nazila Aali, and Mehdi Jaymand. 2016. “Novel Nanostructured Star-Shaped Polythiophene, and Its Electrospun Nanofibers with

Gelatin." *Journal of Polymer Research* 23 (7): 136. https://doi.org/10.1007/s10965-016-1038-x.

Maurice, D. M. 1957. "The Structure and Transparency of the Cornea." *The Journal of Physiology* 136 (2): 263-286.1.

Meek, Keith M., and Carlo Knupp. 2015. "Corneal Structure and Transparency." *Progress in Retinal and Eye Research* 49 (November): 1–16. https://doi.org/10.1016/j.preteyeres.2015.07.001.

Michalak, Monika, Leszek Łatka, Patrycja Szymczyk, and Paweł Sokołowski. 2017. "Computational Image Analysis of Suspension Plasma Sprayed YSZ Coatings." *ITM Web of Conferences* 15: 06004. https://doi.org/10.1051/itmconf/20171506004.

Mohammadzadehmoghadam, Soheila, and Yu Dong. 2019. "Fabrication and Characterization of Electrospun Silk Fibroin/Gelatin Scaffolds Crosslinked With Glutaraldehyde Vapor." *Frontiers in Materials* 6. https://doi.org/10.3389/fmats.2019.00091.

Mohiti-Asli, M., and E. G. Loboa. 2016. "23 - Nanofibrous Smart Bandages for Wound Care." In *Wound Healing Biomaterials*, edited by Magnus S. Ågren, 483–99. Woodhead Publishing. https://doi.org/10.1016/B978-1-78242-456-7.00023-4.

Moreno, Juan, and Rafael Peinado, eds. 2012. "Chapter 19 - Wine Colloids." In *Enological Chemistry*, 323–54. San Diego: Academic Press. https://doi.org/10.1016/B978-0-12-388438-1.00019-4.

Murab, Sumit, Shibu Chameettachal, and Sourabh Ghosh. 2016. "Establishment of an in Vitro Monolayer Model of Macular Corneal Dystrophy." *Laboratory Investigation* 96 (12): 1311–26. https://doi.org/10.1038/labinvest.2016.102.

Nara, Sharda, Shibu Chameettachal, Swati Midha, Sumit Murab, and Sourabh Ghosh. 2016. "Preservation of Biomacromolecular Composition and Ultrastructure of a Decellularized Cornea Using a Perfusion Bioreactor." *RSC Advances* 6 (3): 2225–40. https://doi.org/10.1039/C5RA20745B.

Ning, Wane, Jiwei Huang, Xinlong Ling, and Haitao Lin. 2018. "Modification of Electrospun Silk Fibroin Nanofiber Mats: Using an EDC/NHS Ethanol Solvent." *IOP Conference Series: Materials Science and Engineering* 423 (November): 012068. https://doi.org/10.1088/1757-899X/423/1/012068.

Okhawilai, Manunya, Ratthapol Rangkupan, Sorada Kanokpanont, and Siriporn Damrongsakkul. 2010. "Preparation of Thai Silk Fibroin/Gelatin Electrospun Fiber Mats for Controlled Release Applications." *International Journal of Biological Macromolecules* 46 (5): 544–50. https://doi.org/10.1016/j.ijbiomac.2010.02.008.

Oksa, Maria, Erja Turunen, Tomi Suhonen, Tommi Varis, and Simo-Pekka Hannula. 2011. "Optimization and Characterization of High Velocity Oxy-Fuel Sprayed Coatings: Techniques, Materials, and Applications." *Coatings* 1 (1): 17–52. https://doi.org/10.3390/coatings1010017.

Poddar, Suruchi, Piyush Sunil Agarwal, Ajay Kumar Sahi, Kiran Yellappa Vajanthri, Pallawi, K. N. Singh, and Sanjeev Kumar Mahto. 2019. "Fabrication and Cytocompatibility Evaluation of Psyllium Husk (Isabgol)/Gelatin Composite Scaffolds." *Applied Biochemistry and Biotechnology* 188 (3): 750–68. https://doi.org/10.1007/s12010-019-02958-7.

Poursamar, S. Ali, Alexander N. Lehner, Mahmoud Azami, Somayeh Ebrahimi-Barough, Ali Samadikuchaksaraei, and A. P. M. Antunes. 2016. "The Effects of Crosslinkers on

Physical, Mechanical, and Cytotoxic Properties of Gelatin Sponge Prepared via in-Situ Gas Foaming Method as a Tissue Engineering Scaffold." *Materials Science and Engineering: C* 63 (June): 1–9. https://doi.org/10.1016/j.msec.2016.02.034.

Qi, Yu, Hui Wang, Kai Wei, Ya Yang, Ru-Yue Zheng, Ick Kim, and Ke-Qin Zhang. 2017. "A Review of Structure Construction of Silk Fibroin Biomaterials from Single Structures to Multi-Level Structures." *International Journal of Molecular Sciences* 18 (3): 237. https://doi.org/10.3390/ijms18030237.

Ramos, Marina, Arantzazu Valdés, Ana Beltrán, and María Carmen Garrigós. 2016. "Gelatin-Based Films and Coatings for Food Packaging Applications." *Coatings* 6 (4): 41. https://doi.org/10.3390/coatings6040041.

Reddy, Narendra, Yeanching Tan, Ying Li, and Yiqi Yang. 2008. "Effect of Glutaraldehyde Crosslinking Conditions on the Strength and Water Stability of Wheat Gluten Fibers." *Macromolecular Materials and Engineering* 293 (7): 614–20. https://doi.org/10.1002/mame.200800031.

Ren, Dongwen, Hongfu Yi, Wei Wang, and Xiaojun Ma. 2005. "The Enzymatic Degradation and Swelling Properties of Chitosan Matrices with Different Degrees of N-Acetylation." *Carbohydrate Research* 340 (15): 2403–10. https://doi.org/10.1016/j.carres.2005.07.022.

Rice, William L., Shamaraz Firdous, Sharad Gupta, Martin Hunter, Cheryl Wong Po Foo, Yongzhong Wang, Hyeon Joo Kim, David L. Kaplan, and Irene Georgakoudi. 2008. "Non-Invasive Characterization of Structure and Morphology of Silk Fibroin Biomaterials Using Non-Linear Microscopy." *Biomaterials* 29 (13): 2015–24. https://doi.org/10.1016/j.biomaterials.2007.12.049.

Rockwood, Danielle N., Rucsanda C. Preda, Tuna Yücel, Xiaoqin Wang, Michael L. Lovett, and David L. Kaplan. 2011. "Materials Fabrication from Bombyx Mori Silk Fibroin." *Nature Protocols* 6 (10). https://doi.org/10.1038/nprot.2011.379.

Salvatore, Viviana, Isabella Orienti, Stefano Focaroli, Sandra Durante, Monica Mattioli Belmonte, and Mirella Falconi. 2012. "Cell Adhesion and Proliferation on Gelatin-Ascorbic Acid Scaffold." *Italian Journal of Anatomy and Embryology* 117 (2): 168. https://doi.org/10.13128/IJAE-12279.

Schulz, Dominic, Milko E. Iliev, Beatrice E. Frueh, and David Goldblum. 2003. "In Vivo Pachymetry in Normal Eyes of Rats, Mice and Rabbits with the Optical Low Coherence Reflectometer." *Vision Research* 43 (6): 723–28. https://doi.org/10.1016/S0042-6989(03)00005-1.

Shen, Gaotian, Xingyou Hu, Guoping Guan, and Lu Wang. 2015. "Surface Modification and Characterisation of Silk Fibroin Fabric Produced by the Layer-by-Layer Self-Assembly of Multilayer Alginate/Regenerated Silk Fibroin." *PLOS ONE* 10 (4): e0124811. https://doi.org/10.1371/journal.pone.0124811.

Shi, Weiyun, Qingjun Zhou, Hua Gao, Suxia Li, Muchen Dong, Ting Wang, Yanni Jia, et al. 2019. "Protectively Decellularized Porcine Cornea versus Human Donor Cornea for Lamellar Transplantation." *Advanced Functional Materials* 29 (37): 1902491. https://doi.org/10.1002/adfm.201902491.

Singh, Yogendra Pratap, Ashutosh Bandyopadhyay, and Biman B. Mandal. 2019. "3D Bioprinting Using Cross-Linker-Free Silk–Gelatin Bioink for Cartilage Tissue Engineering." *ACS Applied Materials & Interfaces* 11 (37): 33684–96. https://doi.org/10.1021/acsami.9b11644.

Smith, L. A., and P. X. Ma. 2004. “Nano-Fibrous Scaffolds for Tissue Engineering.” *Colloids and Surfaces. B, Biointerfaces* 39 (3): 125–31. https://doi.org/10.1016/j.colsurfb.2003.12.004.

Song, Ju-Ha, Hyoun-Ee Kim, and Hae-Won Kim. 2008. “Production of Electrospun Gelatin Nanofiber by Water-Based Co-Solvent Approach.” *Journal of Materials Science. Materials in Medicine* 19 (1): 95–102. https://doi.org/10.1007/s10856-007-3169-4.

Tonsomboon, Khaow, and Michelle L. Oyen. 2013. “Composite Electrospun Gelatin Fiber-Alginate Gel Scaffolds for Mechanically Robust Tissue Engineered Cornea.” *Journal of the Mechanical Behavior of Biomedical Materials* 21 (May): 185–94. https://doi.org/10.1016/j.jmbbm.2013.03.001.

Tran, Simon H., Clive G. Wilson, and F. Philipp Seib. 2018. “A Review of the Emerging Role of Silk for the Treatment of the Eye.” *Pharmaceutical Research* 35 (12): 248. https://doi.org/10.1007/s11095-018-2534-y.

Tripathi, Garima. 2017. “Application and Future of Composite Materials: A Review.” *International Journal of Composite and Constituent Materials* 3 (2): 1–4.

Van Vlierberghe, S., G. -J. Graulus, S. Keshari Samal, I. Van Nieuwenhove, and P. Dubruel. 2014. “12 - Porous Hydrogel Biomedical Foam Scaffolds for Tissue Repair.” In *Biomedical Foams for Tissue Engineering Applications*, edited by Paolo A. Netti, 335–90. Woodhead Publishing. https://doi.org/10.1533/9780857097033.2.335.

Varshney, Neelima, Ajay Kumar Sahi, Suruchi Poddar, and Sanjeev Kumar Mahto. 2020. “Soy Protein Isolate Supplemented Silk Fibroin Nanofibers for Skin Tissue Regeneration: Fabrication and Characterization.” *International Journal of Biological Macromolecules* 160 (October): 112–27.

https://doi.org/10.1016/j.ijbiomac.2020.05.090.

Varshney, Neelima, Ajay Kumar Sahi, Kiran Yellappa Vajanthri, Suruchi Poddar, Chelladurai Karthikeyan Balavigneswaran, Arumugam Prabhakar, Vivek Rao, and Sanjeev Kumar Mahto. 2019. "Culturing Melanocytes and Fibroblasts within Three-Dimensional Macroporous PDMS Scaffolds: Towards Skin Dressing Material." *Cytotechnology* 71 (1): 287–303. https://doi.org/10.1007/s10616-018-0285-6.

Wahab, Roswanira, and Naji Mahat. 2016. *Protocols and Methods for Developing Green Immobilized Nanobiocatalysts for Esterification Reactions*.

Wu, Zhengjie, Bin Kong, Rui Liu, Wei Sun, and Shengli Mi. 2018. "Engineering of Corneal Tissue through an Aligned PVA/Collagen Composite Nanofibrous Electrospun Scaffold." *Nanomaterials* 8 (2). https://doi.org/10.3390/nano8020124.

Yin-Guibo, Zhang-Youzhu, Bao-Weiwei, Wu-Jialin, Shi De-bing, Dong Zhi-hui, and Fu Wei-guo. 2009. "Study on the Properties of the Electrospun Silk Fibroin/Gelatin Blend Nanofibers for Scaffolds." *Journal of Applied Polymer Science* 111 (3): 1471–77. https://doi.org/10.1002/app.28963.

Yusoff, Noor Izyan Syazana Mohd, Mat Uzir Wahit, Juhana Jaafar, and Tuck-Whye Wong. 2019. "Structural and Characterization Studies of Insoluble Thai Bombyx Mori Silk Fibroin Films." *Malaysian Journal of Fundamental and Applied Sciences* 15 (1): 18–22. https://doi.org/10.11113/mjfas.v15n2019.1223.

Zhang, Feng, Jian N. Wang, and Bao Q. Zuo. 2010. "Effect of Aqueous Ethanol Treatment on the Electrospun SF Nanofiber Mats." In *2010 4th International Conference on Bioinformatics and Biomedical Engineering*, 1–4. https://doi.org/10.1109/ICBBE.2010.5515644.

Zhang, Lijie, and Thomas J. Webster. 2009. “Nanotechnology and Nanomaterials: Promises for Improved Tissue Regeneration.” *Nano Today* 4 (1): 66–80. https://doi.org/10.1016/j.nantod.2008.10.014.

Zhang, Zheng, Ophir Ortiz, Ritu Goyal, and Joachim Kohn. 2013. *Handbook of Polymer Applications in Medicine and Medical Devices: 13. Biodegradable Polymers*. Elsevier Inc. Chapters.

Zhao, Yuanyuan, and Zhongtao Sun. 2017. “Effects of Gelatin-Polyphenol and Gelatin–Genipin Cross-Linking on the Structure of Gelatin Hydrogels.” *International Journal of Food Properties* 20 (sup3): S2822–32. https://doi.org/10.1080/10942912.2017.1381111.